**DOKUZ EYLÜL UNIVERSITY**
**GRADUATE SCHOOL OF NATURAL AND APPLIED SCIENCES**

# STRUCTURAL AND MECHANICAL PROPERTIES OF Ni BASED NANOCOMPOSITE COATINGS PRODUCED BY ELECTRODEPOSITION TECHNIQUE

**by**
**Onur BARDAKÇIOĞLU**

**October, 2016**
**İZMİR**

# STRUCTURAL AND MECHANICAL PROPERTIES OF Ni BASED NANOCOMPOSITE COATINGS PRODUCED BY ELECTRODEPOSITION TECHNIQUE

**A Thesis Submitted to the**
**Graduate School of Natural and Applied Sciences of Dokuz Eylül University**
**In Partial Fulfillment of the Requirements for the Degree of Master of Science in Department of Nanoscience and Nanoengineering**

**by**
**Onur BARDAKÇIOĞLU**

**October, 2016**
**İZMİR**

**M.Sc THESIS EXAMINATION RESULT FORM**

We have read the thesis entitled **"STRUCTURAL AND MECHANICAL PROPERTIES OF Ni BASED NANOCOMPOSITE COATINGS PRODUCED BY ELECTRODEPOSITION TECHNIQUE"** completed by **ONUR BARDAKÇIOĞLU** under supervision of **ASST. PROF. DR. IŞIL BİRLİK** and we certify that in our opinion it is fully adequate, in scope and in quality, as a thesis for the degree of Master of Science.

Asst. Prof. Dr. Işıl BİRLİK

Supervisor

Asst. Prof. Dr. Funda AK AZEM

Jury Member

Assoc. Prof. Dr. Osman GULLU

Jury Member

Prof.Dr. Ayşe OKUR

Director

Graduate School of Natural and Applied Sciences

## ACKNOWLEDGMENTS

Firstly, I would like to express to my deep and sincere gratitude to my advisor Assist. Prof. Dr. Işıl BİRLİK and co-advisor Assist. Prof. Dr. N. Funda AK AZEM for their excellent guidance, patient supervision and continuous support thought the preparation of this study.

I warmly express my special thanks to my co-worker, Sıdıka YILDIRIM for her support, help, patience and friendship. I wish to extend my sincere thanks to Serhan KÖKTAŞ, Kadir Cihan TEKİN, Dalyan ÖZKAN, Ahmet Çağrı KILINÇ, Tuncay DİKİCİ, Onur ERTUĞRUL, Haydar KAHRAMAN, Ramazan DALMIŞ, Metin YURDDAŞKAL, Oylum ÇOLPANKAN and Orkut SANCAKOĞLU for their collaboration in the laboratory studies and sharing their valuable experiences with me. In addition, I would like to thank Tülay KOÇ DELİCE, Utku TİRİÇ, Bensu BAKIN and Mehmet Bulut ÖZYİĞİT for their invaluable assistance and kind friendship.

The present research was also supported by The Scientific and Technological Research Council of Turkey (TÜBİTAK) with project code 113R023 named as "Production, investigation and industrial utilization of nanocomposite coatings as photoanode applications for cathodic protection systems".

Finally, a special thank goes to my dear family Nevzat BARDAKÇIOĞLU, Hatice BARDAKÇIOĞLU and Ozan BARDAKÇIOĞLU for their concern, confidence and support. The successful completion of this study would not have been possible without their constant love and encouragement.

Onur BARDAKÇIOĞLU

**STRUCTURAL AND MECHANICAL PROPERTIES OF Ni BASED NANOCOMPOSITE COATINGS PRODUCED BY ELECTRODEPOSITION TECHNIQUE**

## ABSTRACT

Main idea of this thesis is to fabricate Ni based nanocomposite coatings by electrodeposition method and to investigate effects of current density, particle size and particle concentration on the structure and mechanical properties of Ni based nanocomposite coatings.

First of all, titanium dioxide, zinc oxide and chromium oxide nanoparticles were synthesized by sol-gel technique using titanium tetraisopropoxide, zinc acetate dihydrate and chromium nitrate nonahydrate as the precursors, respectively. Structural characterization and particle size measurements of the nanoparticles were examined by using X-Ray Diffraction (XRD) and particle size analyzer, respectively.

Afterwards, pure Ni and Ni based nanocomposite coatings were produced on steel substrate by electrodeposition method. Crystalline structure of the produced nanocomposite coatings were performed by XRD and surface morphologies were investigated using Scanning Electron Microscope (SEM) with an Energy Dispersive Spectrometer (EDS) system attachment. Nevertheless, mechanical properties of the pure Ni and Ni based nanocomposite coatings such as hardness and elastic modulus were performed under 150 mN applied load by IBIS nanoindentation system. It was observed that the incorporation of nanoparticles enhanced the mechanical properties of Ni matrix.

**Keywords:** Nanoparticle, sol-gel technique, nickel coating, nanocomposite, electrodepostion, nanoindentation.

# ELEKTROÇÖKTÜRME TEKNİĞİ İLE ÜRETİLEN Ni ESASLI NANOKOMPOZİT KAPLAMALARIN YAPISAL VE MEKANİK ÖZELLİKLERİ

## ÖZ

Bu çalışmanın ana fikri elektroçöktürme yöntemiyle Ni esaslı nanokompozit kaplamalar üretmek ve Ni esaslı nanokompozit kaplamaların yapısal ve mekanik özelliklerinin üzerine akım yoğunluğu, partikül boyutu ve partikül konsantrasyonunun etkisini incelemektir.

İlk olarak, titanyum dioksit, çinko oksit ve krom oksit nanopartikülleri sırasıyla titanyum tetra izopropoksit, çinko asetat dihidrat ve krom nitrat nonahidrat başlangıç kimyasalları kullanılarak sol-jel yöntemiyle sentezlenmiştir. Nanopartiküllerin yapısal karakterizasyonları ve partikül boyut ölçümleri sırasıyla X ışını difraktometresi (XRD) ve partikül boyut analizi cihazları kullanılarak incelenmiştir.

Daha sonra, saf nikel ve Ni esaslı nanokompozit kaplamalar elektroçöktürme yöntemiyle çelik altlık üzerine üretilmiştir. Üretilen nanokompozit kaplamaların kristal yapıları XRD cihazıyla analiz edilmiştir ve yüzey morfolojileri enerji saçınım spektrometresi (EDS) entegreli taramalı elektron mikroskobu (SEM) cihazında incelenmiştir. Bunun yanında saf Ni ve Ni esaslı nanokompozit yapılara ait sertlik ve elastisite modülü gibi mekanik özellikler 150 mN yük altında IBIS nanoindentasyon cihazı kullanılarak belirlenmiştir. Nanopartiküllerin ilave edilmesiyle Ni matriksin mekanik özelliklerinin geliştiği gözlenmiştir.

**Anahtar kelimeler:** Nanopartikül, sol-jel yöntemi, nikel kaplama, nanokompozit, elektroçöktürme, nanoindentasyon.

**CONTENTS**

**Page**

## LIST OF FIGURES

**Page**

## LIST OF TABLES

**Page**

# CHAPTER ONE
# INTRODUCTION

Nanotechnology is the study, design, creation, synthesis, manipulation and application of functional materials, devices, and systems through control of matter at the nanometer scale (1–100 nanometers, one nanometer being equal to $1 \times 10^{-9}$ of a meter), that is, at the atomic and molecular levels, and the exploitation of novel phenomena and properties of matter at that scale (Salamanca-Buentello, Persad, Martin, Daar & Singer, 2005).

The sol-gel process, a frequently used technique for the preparation of nanoparticles, involves the development of networks through an arrangement of colloidal suspension (sol) and gelation to form a system in continuous liquid phase (gel). A sol is basically a dispersion of colloidal particles (1–100 nm) in a liquid and a gel is an interconnected rigid network with pores of sub-micron dimensions and polymeric chains (Singh et al., 2014).

Nickel electroplating is a commercially important and versatile surface-finishing process. Its commercial importance may be judged from the amount of nickel in the form of metal and salts consumed annually for electroplating, now roughly 100.000 metric tons worldwide, as well as its versatility from its many current applications (Di Bari, 2000).

Nickel is one of the most important metals applied via electrodeposition (Sadiku-Agboola, Sadiku, Ojo, Akanji & Biotidara, 2011). However, the nickel-deposited surface shows low surface mechanical properties and to improve this electrodeposition of Ni with non-metal was investigated regularly. The electro-co-deposition of Ni with second phase hard inert particles such as metal oxides, metal carbides, nitrides, borides ($TiO_2$, $ZrO_2$, $SiO_2$, $Al_2O_3$, $Cr_2O_3$, SiC, WC, TiC, $Cr_3C_2$, $Si_3N_4$, BN, and ZrB), carbon nanotube (CNTs), and diamond are generally used in composite coating to improve properties such as hardness, wear resistance, and corrosion resistance (Parida, Chaira, Chopkar & Basu, 2011). It is known that in severe plastic deformation (SPD)

processing, a steady-state grain size is eventually reached at ultra-high strains that limit the achievable level of grain refinement. This limit is controlled by the mobility of low- and high-angle grain boundaries. The introduction of second-phase particles, which effectively pin grain boundaries, is a method for decreasing the limiting grain size, allowing an increase in strength (Nikulin, Kipelova, Malopheyev & Kaibyshev, 2012).

In the present study incorporation of ceramic particles has been adopted to improve the properties of electrodeposited Ni based nanocomposite coatings.

The structure of the thesis consists of five different parts in addition to this chapter which are summarized below:

Chapter 2 is a literature review, including nanomaterials and production techniques.

Chapter 3 is a literature review, including Ni coating, different types of Ni coating baths, nanocomposite coatings and Ni matrix nanocomposite coatings production techniques.

Chapter 4 is on the experimental work conducted, including production of nanoparticles, preparation of the substrate, production of electrodeposited pure Ni and Ni matrix nanocomposite coatings, characterization techniques and nanoindentation studies.

Chapter 5 presents results and discussions, including XRD and particle size measurements of nanoparticles and XRD, SEM, nanoindentation results of pure Ni and Ni matrix nanocomposite coatings.

Chapter 6 reviews the main conclusions of the study.

# CHAPTER TWO
# THEORITICAL BACKGROUND

## 2.1 Nanoscience and Nanotechnology

The prefix “nano”, derived from the Greek “nanos” signifying “dwarf”, is becoming increasingly common in scientific literature. "Nano" is now a popular label for much of modern science, and many “nano-“ words have recently appeared in dictionaries, including: nanometer, nanoscale, nanoscience, nanotechnology, nanostructure, nanotube, nanowire, and nanorobot. Many words that are not yet widely recognized are used in respected publications, such as Science and Nature. These include nanoelectronics, nanocrystal, nanovalve, nanoantenna, nanocavity, nanoscaffolds, nanofibers, nanomagnet, nanoporous, nanoarrays, nanolithography, nanopatterning, nanoencapsulation, etc (Buzea, Pacheco & Robbie, 2007).

The word “nanotechnology” was introduced for the first time into a scientific world by N. Taniguchi at the international conference on industrial production in Tokyo in 1974 in order to describe the super thin processing of materials with nanometer accuracy and the creation of nano-sized mechanisms.

Ideas of nanotechnological strategy, which were put forward by Feynman, were developed by E. Drexler in his book “Vehicles of creation: the arrival of the nanotechnology era” published in 1986.

In the second half of 1980s to the early 1990s a number of important discoveries and inventions was made, which created an essential impact on the further development of nanotechnology. Since then, a considerable intensification of nanotechnological researches and designs is underway, the number of publications on nanotechnological subjects increases sharply, practical application of nanotechnology expands; project financing in nanotechnology increases significantly, as well as the number of organizations and countries involved in it (Tolochko, 2009).

Since 2000, awareness of nanotechnology among environmental activists, regulators, and lawmakers has been on the rise. Environmental organizations have expressed fears about the potential ecological and health consequences of mainstream nanotechnology, and have called for increased research into safety of nanoparticles (Melnik & Shagalina, 2011).

Nanomaterials are materials that have structural components smaller than 1 micrometer in at least one dimension. While the atomic and molecular building blocks (~0.2 nm) of matter are considered nanomaterials, examples such as bulk crystals with lattice spacing of nanometers but macroscopic dimensions overall, are commonly excluded (Buzea et al., 2007). Classificitaion of nanomaterials were given in Table 2.1 (Alagarasi, 2011).

Table 2.1 Classification of nanomaterials (Alagarasi, 2011)

| **Nanomaterial dimension** | **Examples** |
|---|---|
| One dimension < 100 nm | Surface films, layers, coatings |
| Two dimension < 100 nm | Strands, fibers, nanotubes, nanowires |
| Three dimension < 100 nm | Nanoparticles, nanoshells, nanorings |

A nanoparticle is the most fundamental component in the fabrication of a nanostructure, and is far smaller than the world of everyday objects that are described by Newton's laws of motion, but bigger than an atom or a simple molecule that are governed by quantum mechanics (Horikoshi & Serpone, 2013).

The transition from microparticles to nanoparticles can lead to a number of changes in physical properties. Two of the major factors in this are the increase in the ratio of surface area to volume, and the size of the particle moving into the realm where quantum effects predominate.

The increase in the surface-area-to-volume ratio, which is a gradual progression as the particle gets smaller, leads to an increasing dominance of the behavior of atoms on the surface of a particle over that of those in the interior of the particle. This affects both the properties of the particle in isolation and its interaction with other materials. High surface area is a critical factor in the performance of catalysis and structures such

as electrodes, allowing improvement in performance of such technologies as fuel cells and batteries. The large surface area of nanoparticles also results in a lot of interactions between the intermixed materials in nanocomposites, leading to special properties such as increased strength and/or increased chemical/heat resistance (Holister, Weener, Vas & Harper, 2003).

In general, the size of a nanoparticle spans the range between 1 and 100 nm. Metallic nanoparticles have different physical and chemical properties from bulk metals (e.g., lower melting points, higher specific surface areas, specific optical properties, mechanical strengths, and specific magnetizations), properties that might prove attractive in various industrial applications (Horikoshi & Serpone, 2013).

Nanoparticles have been used for a very long time, probably the earliest use being in glazes for early dynasty Chinese porcelain. A Roman cup, called the Lycurgus cup, used nanosized gold clusters to create different colors depending on whether it was illuminated from the front or the back. The cause of this effect was not, of course, known to those who exploited it. Carbon black is the most famous example of a nanoparticulate material that has been produced in quantity for decades (Holister et al., 2003).

## 2.2 Synthesis of Nanomaterials

There are two approaches to the synthesis of nanomaterials and the fabrication of nanostructures: top-down and bottom-up.

The top-down method is the method of breaking up a solid substance; it can be sub-divided into dry and wet grinding. A characteristic of particles in grain refining processes is that their surface energy increases, which causes the aggregation of particles to increase also. In the dry grinding method the solid substance is ground as a result of a shock, a compression, or by friction, using such popular methods as a jet mill, a hammer mill, a shearing mill, a roller mill, a shock shearing mill, a ball mill, and a tumbling mill (Horikoshi & Serpone, 2013).

Bottom-up approach refers to the build-up of a material from the bottom: atom-by-atom, molecule-by-molecule, or cluster-by-cluster. Although the bottom-up approach is nothing new, it plays an important role in the fabrication and processing of nanostructures and nanomaterials. Bottom-up approach also promises a better chance to obtain nanostructures with less defects, more homogeneous chemical composition, and better short and long range ordering. This is because the bottom-up approach is driven mainly by the reduction of Gibbs free energy, so that nanostructures and nanomaterials such produced are in a state closer to a thermodynamic equilibrium state (Cao, 2004). The other preparation methods of nanomaterials were given in Fig. 2.2.

Attrition or milling is a typical top-down method in making nanoparticles, whereas the colloidal dispersion is a good example of bottom-up approach in the synthesis of nanoparticles. Lithography may be considered as a hybrid approach, since the growth of thin films is bottom-up whereas etching is top-down, while nanolithography and nanomanipulation are commonly a bottom-up approach. Both approaches play very important roles in modern industry and most likely in nanotechnology as well (Cao, 2004). Various preparation techniques for nanomaterials classified according to other dimensions are summarized in Figure 2.1.

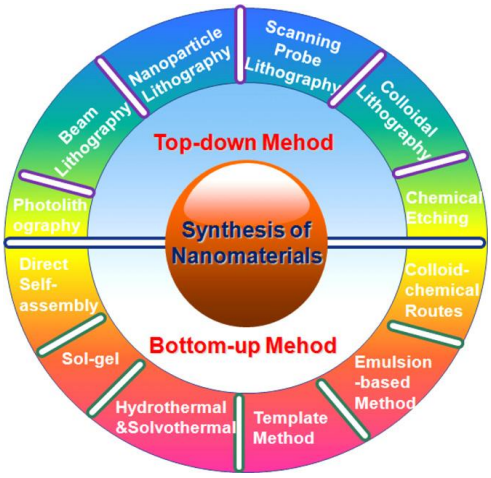


Figure 2.1 Schematic illustration of the synthesis method of nanomaterials (Qiao, Liu & Lu, 2011).

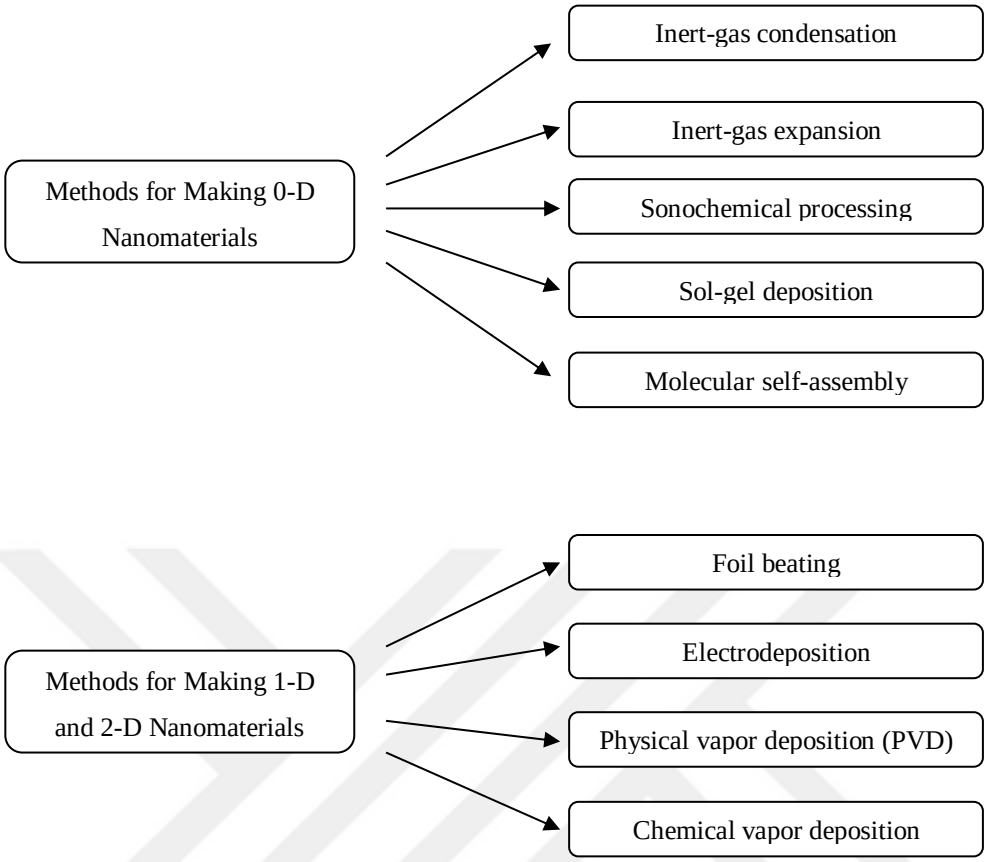


Figure 2.2 Typical synthetic methods for nanomaterials(Schodek, Ferreira & Ashby, 2009).

### *2.2.1 Inert-gas Condensation*

Inert-gas condensation (IGC) is a bottom-up approach to synthesizing nanostructured materials, which involves two basic steps. The first step is the evaporation of the material and the second step involves a rapid controlled condensation to produce the required particle size. Figure 2.3 shows a schematic of a typical apparatus used for inert-gas condensation method (Koch, 2006).

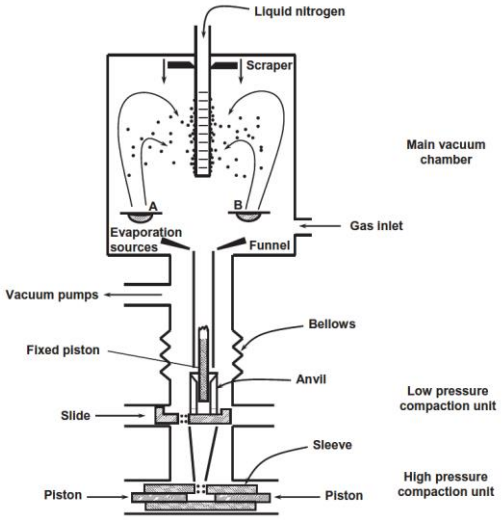


Figure 2.3 Schematic of the inert-gas condensation chamber for the synthesis of nanostructured materials (Koch, 2006).

### *2.2.2 Inert-gas (free-jet) Expansion*

Free-jet expansions have been used by chemists, physicists, and engineers for many years in a variety of applications, including studies of photodissociation, elastic, inelastic, and reactive scattering in crossed molecular beams, the preparation of jet-cooled molecules for high-resolution spectroscopy, the formation of van der Waals cluster molecules, the measurement of rate constants for ionmolecule quenching or charge transfer reactions at very low temperatures, and studies of aerodynamics (Figure 2.4) (Creasey et al., 1997; Schodek et al., 2009).

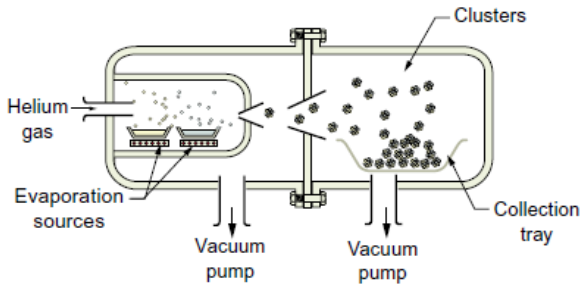


Figure 2.4 Cluster formation by vapor phase expansion from an oven source (Schodek et al., 2009).

### *2.2.3 Sonochemical Processing*

Sonochemistry is one of the earliest techniques used to prepare nanomaterials. Sonochemistry is the research area in which molecules undergo a chemical reaction due to the application of powerful ultrasound radiation (20 kHz-10 MHz). The physical phenomenon responsible for the sonochemical process is acoustic cavitation (Figure 2.5) (Qiao et al., 2011; Schodek et al., 2009).

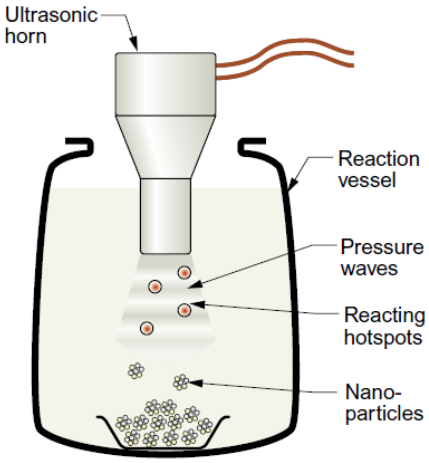


Figure 2.5 Sonochemical processing (Schodek et al., 2009).

### *2.2.4 Sol-gel Process*

This process involves the evolution of inorganic networks through the formation of a colloidal suspension which is called sol and gelation of the sol to form a network in a continuous liquid phase which is denoted as gel. Three reactions generally describe the sol-gel process: (1) hydrolysis reaction, (2) alcohol condensation process, and (3) water condensation process (Qiao et al., 2011).Ultrafine particles, nanothickness films, and nanoporous membranes can be made by sol-gel processing (Schodek et al., 2009). This method will be interviewed in detail on section 2.4.

### *2.2.5 Molecular Self-assembly*

One of the major technological challenges in nanoscience and nanotechnology is the self-assembly of tiny nano-building units (nanokits and nanoparts) into larger

organized conformations and geometrical architectures for device applications. Self-assembly phenomena have been used both to form templates for fabricating nanostructures and to assemble the nanostructure itself. Self-assembled processes are molecular processes (Figure 2.6) (Qiao et al., 2011; Schodek et al., 2009).

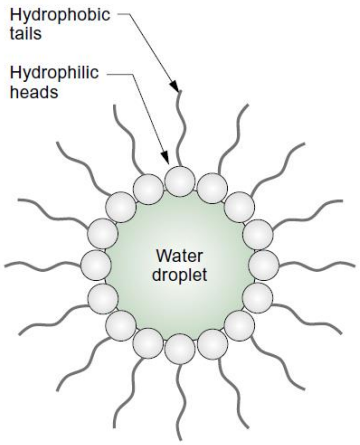


Figure 2.6 Self-assembly of nanoclusters. The enclosed droplet can be spherical or cylindrical. Reaction within it generates a nanoparticle or nanorod(Schodek et al., 2009).

### *2.2.6 Foil Beating*

Gilding is the art of applying gold leaf to a surface. It was known to the ancients, is mentioned in the Old Testament, and was described by Herodotus in 420 BC. Gold is an expensive material; there are obvious incentives to use as little of it as possible. Gold leaf is made by beating the metal to a uniformly thin foil, roughly 100 nm thick (Figure 2.7). It is applied by smoothing it onto the adhesivecoated surface of the object to be gilded. There are less labor-intensive ways to make thin films. Electrodeposition is one, and it is one able to create nanoscale structures as well (Schodek et al., 2009).

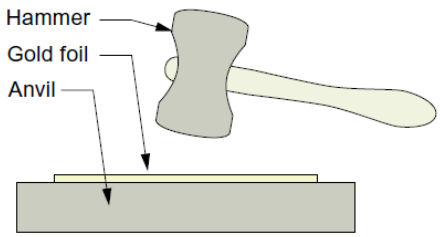


Figure 2.7 Beating of gold leaf (Schodek et al., 2009).

### *2.2.7 Electrodeposition*

Electrodeposition of metallic films (commonly known as electroplating) has long been known and used for preparing metallic mirrors and corrosion-resistant surfaces, among other things. In its simplest form, the electroplating or electrodeposition bath consists of an electrolyte containing metal ions (for example, $NiSO_4$ solution for the deposition of nickel), an electrode or substrate on which the deposition is desired, and a counter electrode. When a current flows through the electrolyte, the cations and anions move toward the cathode and anode, respectively, and may deposit on the electrodes after undergoing a charge transfer reaction. Suppose nickel is to be electrodeposited (Pandey, Chandra & Sahu, 1996). This method will be interviewed in detail on section 3.5.1.

### *2.2.8 Physical Vapor Deposition (PVD)*

PVD is a process of transferring growth species from a source or target and deposit them on a substrate to form a film (Figure 2.8). The process proceeds atomistically and mostly involves no chemical reactions (Cao, 2004; Schodek et al., 2009).

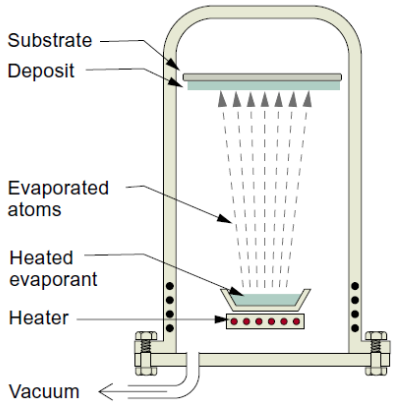


Figure 2.8 Physical vapor deposition (PVD). Material, evaporated by heating, by ion bombardment, or by laser ablation, is deposited on a substrate target. The deposited layer can be of nano thickness (Schodek, Ferreira et al. 2009).

### *2.2.9 Chemical Vapor Deposition (CVD)*

CVD is a well known process in which a solid is deposited on a heated surface via a chemical reaction from the vapor or gas phase (Figure 2.9). CVC reaction requires activation energy to proceed. This energy can be provided by several methods. In thermal CVD the reaction is activated by a high temperature above 900°C. In plasma CVD, the reaction is activated by plasma at temperatures between 300 and 700°C. In laser CVD, pyrolysis occurs when laser thermal energy heats an absorbing substrate. In photo-laser CVD, the chemical reaction is induced by ultra violet radiation which has sufficient photon energy, to break the chemical bond in the reactant molecules. In this process, the reaction is photon activated and deposition occurs at room temperature (Rajput, 2015; Schodek et al., 2009).

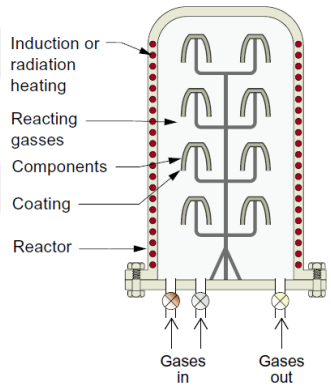


Figure 2.9 Chemical vapor deposition (CVD) (Schodek, Ferreira et al. 2009).

## 2.3 Sol-Gel Processing

Sol-gel processing is a wet chemical route for the synthesis of colloidal dispersions of inorganic and organic-inorganic hybrid materials, particularly oxides and oxide-based hybrids (Cao, 2004). Sol-gel chemistry has been investigated extensively since the mid-1970s, when sol-gel reactions were shown to produce a variety of inorganic networks that can be formed from metal alkoxide solutions (Nogami & Moriya, 1980). Sol–gel process can occur under extraordinary mild conditions, so it can be used to obtain products of various sizes, shapes and formats (e.g. fibers, films, monoliths and monosized particles) (Kumar, Malik, Tewary & Singh, 2008). Sol–gel technology has

found ever increasing applications in development of new materials for catalysis (Schubert, 1994), chemical sensors (Wolfbeis, Reisfeld & Oehme, 1996), membranes (Brinker et al., 1995), fibers (Zeng, Qiu & Huang, 2001), optical gain media (Gvishi, Narang, Ruland, Kumar & Prasad, 1997), photochromic and non linear applications (Levy & Esquivias, 1995), solid state electrochemical devices (Dunn, Farrington & Katz, 1994), in diverse range of scientific and engineering fields, such as ceramic industry, nuclear field industry (Scherer & Brinker, 1990) and electronic industry (Kumar et al., 2008). The inherent advantages of sol–gel process are summarized as (Mackenzie & Ulrich, 1988):

- Better homogeneity-from raw materials.
- Better purity-from raw materials.
- Lower temperature of preparation.
- Good mixing for multi-component systems.
- Control of particle size, shape and properties.
- Better products from special properties of gel.
- Special products such as films.
- New non-crystalline solids outside the range of normal glass formation.

The sol-gel chemical process is self-described in the definition of a sol, a gel, and a summary of the process in which a sol evolves into a gel (Brinker & Scherer, 2013). A sol is a colloidal dispersion of small particles in a liquid; a gel is usually a substance composed of a continuous network encompassing a continuous liquid phase (Brinker, 1988). Sol-gel reactions promote the growth of colloidal particles (sol) and their subsequent network formation (gel) through the hydrolysis and condensation reactions of inorganic alkoxide monomers. The precursors for synthesizing these colloids consist of a metal or metalloid element surrounded by various reactive ligands. Metal alkoxides are most popular because they react readily with water (Young, 2002).

Sol-gel process is used for production of nanoparticles. For example, Bagheri and his friends synthesized $TiO_2$ nanoparticles via sol-gel method. In this study, Anatase $TiO_2$ nanoparticles were synthesized with and without water-soluble egg white

proteins (albumin) by the sol-gel method. From the results, it is clear that synthesized $TiO_2$ nanoparticles exhibited the anatase structure (Bagheri, Shameli & Abd Hamid, 2012). In another study, Dalvandi and Ghasemi synthesized $TiO_2$ nanoparticles by sol-gel method. In their study, tetra-n-butyl orthotitanate was considered as metal precursor and deionized water used as diluents solution. According to their results, $TiO_2$ nanoparticles were successfully synthesized at different calcination temperatures (Dalvandi & Ghasemi, 2013).

Kolekar and his colleagues synthesized ZnO nanoparticles by sol-gel method. In the present study, ZnO nanoparticles have been successfully synthesized at room temperature (Kolekar, Yadav, Bandgar & Deshmukh, 2011). In another study, Ba-Abbad and his colleagues investigated the effect of process parameters on the size of ZnO nanoparticles synthesized via the sol-gel technique. In their study, zinc acetate dehydrate, oxalic acid dehydrate, ammonia solution (%28), sodium hydroxide, hydrochloric acid and absolute ethanol were used as chemicals. From the results, the average crystal and particle size of ZnO nanoparticles increased when the molar ratio of the starting was increased with the reaction pH and the calcination temperature greater than the optimal conditions. The less effect of the molar ratio on the size of the ZnO nanoparticles in comparison with other parameters was also obtained (Ba-Abbad, Kadhum, Mohamad, Takriff & Sopian, 2013).

Aghaie-Khafri and Kakaei Lafdani synthesized $Cr_2O_3$ nanoparticles via sol-gel process. According to their research $Cr_2O_3$ nanoparticles with high surface area have been successfully obtained via EDTA as a chelating agent. (Aghaie-Khafri & Lafdani, 2012). In another study, Karimian and his colleagues synthesized $Cr_2O_3$ nanoparticles by sol-gel method. $CrCl_3$, NaOH, purified soybean oil, Tween 80 and distilled water were used in their study (Karimian, Piri & Davarpanah, 2014).

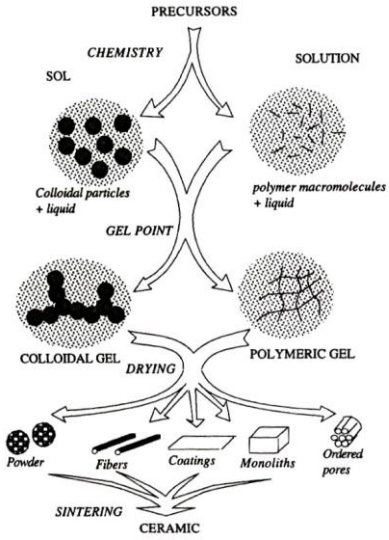


Figure 2.10 Simplified chart of sol-gel process (Pierre, 2013).

### *2.3.1 Hydrolysis and Condensation*

Hydrolysis is the deprotonation of a solvated M cation and it consists in the loss of a proton by one or more of the water molecules that surrounds the M during hydrolysis process. As a consequence, the aqua ligand molecule, $H_2O$ that is bonded to the metal is either transformed into a hydroxo ligand, $OH^-$, if only one proton leaves, or into an oxo ligand $O^{-2}$, if two protons separates. In alkoxides hydrolysis process, the alkoxy groups (OR) are replaced either by hydroxo ligands (OH) or oxo ligands (O) (Pierre, 2013).

This reaction is influenced by various factors including,

- the nature of the alkyl group,
- the nature of the solvent,
- the concentration of each specie in the solvent,
- the water to alkoxide molar ratio and the temperature.

In the first hydrolysis reaction, reaction (2.1), a first hydroxo ligand substitutes an alkoxy group.

$$M(OR)_z + H_2O \Longrightarrow M(OH)(OR)_{z-1} + ROH \qquad (2.1)$$

After hydrolysis, condensation reaction occurs to form a polynuclear complex. Condensation, in aqueous solutions, is the result of either an olation or an oxolation reaction. In either case, one must be quite careful as the oxygen present sometimes speeds the reaction to a point where it becomes necessary to work in the neutral atmosphere of argon in order to control it (Pierre, 2013).

After hydrolysis, condensation reaction occurs to form a polynuclear complex consisting of two metal atoms. Condensation, in aqueous solutions, is the result of either an olation or an oxolation reaction. In either case, one must be quite careful as the oxygen present sometimes speeds the reaction to a point where it becomes necessary to work in the neutral atmosphere of argon in order to control it (Pierre, 2013). In the first case, transfer of the H to an OR ligand according to the reaction below (olation process);

$$2M(OR)_{x-1}(OH) \longrightarrow M_2O(OR)_{2x-3}OH + ROH \text{ (Condensation)} \qquad (2.2)$$

In the second case, transfer of the H to an OH group according to Reaction (2.3), condensation is called oxolation.

$$2M(OR)_{x-1}(OH) \longrightarrow M_2O(OR)_{2x-3}+H_2O \quad \text{(Condensation)} \qquad (2.3)$$

Hydrolysis and condensation both keep on going thus gradually building up a tridimensional network that, at the end, often forms a solid phase. This process is accelerated by heat as the rate of the both reactions increases together with the temperature. Since the kinetics of hydrolysis and condensation, and hence the overall reaction and the type of polymers formed, depends on the pH, a great variety of materials with different structures can be obtained. These include linear polymers as well as dense colloidal particles and smaller ones with more or less weakly bonded cross-linked clusters of polymers (Pierre, 2013).

### *2.3.2 Gelation*

Gelation is a process according to which a sol or solution, transforms to a gel. It consists of establishing links between the sol particles or the solution molecules so as to form 3-dimensional solid network.

Gelation occurs when the extent of polymerization reactions ξ reaches a critical value ξc. This precise critical stage, when for the first time a polymer of infinite size is formed by comparison with the molecular scale, defines the gel point. In a practical manner, at this point the product resulting from polymeric condensations transforms suddenly from a viscous liquid to a material with elastic properties. In the liquid state a viscosity can be measured and its value increases towards infinity when coming near the gel point. In this model of gelation, called the Flory- Stockmayer model (or FS model), the infinite polymer is built by the successive addition of branches, all of which are constructed from the initial monomers (Pierre, 2013).

### *2.3.3 Drying and Sintering*

Drying is irreversible transformation of the gel which is composed of a solid network and liquid matrix. This capillary mechanism explains well the reproducible adsorption hysteresis curves of water in silica gels. This mechanism can be summarized as follows:

- Evaporation creates a liquid vapor meniscus at the exit of pores in the gel.
- This induces a hydrostatic tension in the liquid, which is balanced by an axial compression on the solid.
- The latter compression makes the gel shrink.
- As a result of shrinkage, more liquid is fed to the menisci at the exit of the gel pores, where it is evaporated and so on (Pierre, 2013).

Simultaneously with the transformations of a gel to ceramics, the specific surface area of sol-gel materials decreases during thermal treatments. The progressive

elimination of the porosity is an evolution named sintering. In terms of thermodynamics, sintering originates from the specific surface area Sa of a porous material, which introduce a positive contribution Gs due to the surface of pores, to the Gibbs free energy of a material (Pierre, 2013):

$$G_s = \gamma S_\alpha \tag{2.4}$$

Sol-gel ceramics just after drying and even after heat treatments at intermediate temperatures often have a very high specific surface area and an extremely small grain size. Hence, both sintering and grain growth tend to be vigorous (Schwartz, 1997).

# CHAPTER THREE
# NICKEL AND NICKEL MATRIX NANOCOMPOSITE COATINGS

## 3.1 Nickel Coating

Applying a coating on the surface is a method to improve the surface properties (Baghery, Farzam, Mousavi & Hosseini, 2010). Nickel is one of the most important metals applied by electro-deposition. The plate is used mainly as a bright coating underneath a much thinner chromium electroplate to provide a highly bright, shining and corrosion-protective finish for articles of steel, brass, zinc die castings, chemically metalized plastics, and, to a much smaller extent, for coatings on aluminium and magnesium alloys (Sadiku-Agboola et al., 2011) .

The electrodeposition of nickel was first described in 1837. G. Bird electrolysed solutions of nickel chloride or sulphate for some hours and so obtained a crust of metallic nickel on a platinum electrode (Dennis & Such, 1993; Di Bari, 2000). In 1840, the first patent for commercial nickel plating was granted to J. Shore of England who specified a solution of nickel nitrate. Soon afterwards a number of investigators published the results of their experiments (Dennis & Such, 1993).

Professor Oliver P. Watts at the University of Wisconsin, aware of most of these developments, formulated an electrolyte in 1916 that combined nickel sulfate, nickel chloride, and boric acid and optimized the composition of the nickel electroplating solution (Watts & Deverter, 1916). The advantages of his hot, high-speed formula became recognized and eventually led to the elimination of nickel ammonium sulfate and other proprietary solutions. Today the Watts solution is widely applied, and its impact on the development of modern nickel electroplating technology cannot be overstated (Di Bari, 2000). Decorative nickel plating solutions are variations of the original Watts formulation, the main difference being the presence in solution of organic and certain metallic compounds to brighten and level the nickel deposit. Because of his use of organic additives like benzene and naphthalene di- and trisulfonic acids, Schlotter’s decision to market a bright nickel plating solution in 1934

is a milestone in the commercial development of decorative nickel plating (Max, 1934).

In the recent time, nickel-based alloys find extensive applications primarily in critical components of aerospace engines and gas turbines. Owing to their admirable properties such as fatigue strength, thermal stability and resistance to corrosion under severe environment, in fact, about 50% by weight of aero-engine is made up of nickel-based alloys. Other applications include petrochemical plants, marine equipment, food processing equipment, pollution control apparatus and nuclear reactors. However, these materials pose a considerable challenge during machining due to their low thermal conductivity, high work hardening tendency, hot hardness, chemical affinity towards tool material, and presence of abrasive carbide particles in their microstructure (Thakur & Gangopadhyay, 2016).

## 3.2 Nickel Electroplating Solutions

### *3.2.1 Watts Bath*

The majority of nickel plating solutions, particularly those used for decorative plating, are based on the 'Watts' formulation developed by Professor Oliver P. Watts in 1916. The Watts electrolyte combines nickel sulphate, nickel chloride and boric acid. While the proportions may vary according to the application, a typical formulation together with operating parameters is given in Table 3.1 (Rose & Whittington, 2002).

Table 3.1 Typical formula and operating conditions for Watts nickel electroplating solutions

| | |
|---|---|
| Nickel Sulphate ($NiSO_4.6\ H_2O$) | 240 - 300 g $L^{-1}$ |
| Nickel Chloride ($NiCl_2.6\ H_2O$) | 30 - 90 g $L^{-1}$ |
| Boric Acid ($H_3BO_3$) | 30 - 45 g $L^{-1}$ |
| Temperature | 40 - 60 °C |
| pH | 3.5 - 4.5 |
| Cathode Current Density | 2 - 7 A $dm^{-2}$ |
| Deposition Rate | 25 - 85 μm $h^{-1}$ |

The nickel sulphate is the primary source of nickel ions ($Ni^{++}$) with nickel chloride a contributing source (Rose & Whittington, 2002). This salt is the least expensive salt of nickel with a stable anion that is not reduced at the cathode, oxidized at the anode or volatized. It is also highly soluble and readily available commercially (Sadiku-Agboola et al., 2011).

A principal function of the chloride ion is to improve anode dissolution by reducing polarization. It improves the cathode efficiency and also improves the electrical conductivity of the solution. A small amount of nickel chloride is usually added to nickel sulfamate solutions to minimize anode passivity, especially at high current densities (Sadiku-Agboola et al., 2011).

Boric acid is a buffer and has the major function of controlling the pH of the solution. Due to the cathode efficiency being less than 100% there is a tendency for the pH to increase as some hydrogen ions ($H^{+}$) are discharged to liberate hydrogen gas. Regular additions of sulphuric acid are therefore required to adjust the pH. Boric acid limits the effect on the pH resulting from the discharge of hydrogen ions, thereby, simplifying pH control. The mechanism by which boric acid operates is complex, but it is generally understood that it exists in solution as a mixture of borate ions and non-ionised boric acid. When hydrogen is discharged some boric acid will ionise to replace the hydrogen ions lost and so the pH change is limited. At the same time, borate ions form. When acid is added to adjust the pH, these borate ions combine with hydrogen ions to reform boric acid. Boric acid is therefore only lost through dragout or other solution losses (Rose & Whittington, 2002).

Carriers are usually aromatic organic compounds containing sulphur. Examples are benzene sulphonic acid, 1,3,6-naphthalene sulphonic acid (sodium salt), p-toluene sulphonamide, saccharin and allyl sulphonic acid. The major function of carriers is to refine the grain structure and to provide some increased lustre compared with additive-free solutions. In combination with carriers, brighteners produce brilliant deposits with good ductility and levelling properties over a broad current density range. There are a wide range of brighteners used (generally supplied as proprietary mixtures).

Compounds include formaldehyde chloral hydrate, o-sulpho benzaldehyde, allyl sulphonic acid, 2-butyne-1, 4-diol, thiourea, coumarin and many others. Brighteners are generally present in very low concentrations and are consumed by electrolysis. They therefore need to be replenished on a regular basis in order to maintain the desired brightness (Rose & Whittington, 2002).

### *3.2.2 Nickel Sulfamate Bath*

Nickel sulphamate solutions are chiefly used for the deposition of functional coatings or for electroforming. For such applications the low stress which can be achieved without the use of addition agents, the high deposition rates and desirable deposit properties offset their higher cost. Typical composition and operating conditions are shown in Table 3.2 (Rose & Whittington, 2002).

Table 3.2 Typical composition and operating conditions for nickel sulphamate electroplating solutions

| | |
|---|---|
| Nickel Sulphamate ($Ni(NH_2SO_3)_2.4H_2O$) | 300 - 450 g $L^{-1}$ |
| Nickel Chloride ($NiCl_2.6\ H_2O$) | 0 - 30 g $L^{-1}$ |
| Boric Acid ($H_3BO_3$) | 30 g $L^{-1}$ |
| Temperature | 40 - 60 °C |
| pH | 3.5 - 4.5 |
| Cathode Current Density | 2 - 15 A $dm^{-2}$ |
| Deposition Rate | 25 - 180 μm $h^{-1}$ |

### *3.2.3 Other Types of Electrolytes for Nickel Coating Process*

*The fluoborate bath* can be operated over a wide range of nickel concentrations, temperature, and current density and is relatively simple to control (Roehl & Wesley, 1950). The fluoborate anion is corrosive, however, and some materials that contact the solution are chemically attacked. The mechanical and physical properties of deposits from a fluoborate bath are similar to those fromWatts solutions. The major advantage is that electrodeposition from a nickel fluoborate solution can be performed at high current density (Di Bari, 2000).

*Hard nickel bath* developed especially for functional applications, this solution is applied where controlled hardness, improved abrasion resistance, greater tensile strength, and good ductility are required without using sulfur-containing organic addition agents (Wesley & Roehl, 1942). Close control of pH, temperature, and current density is necessary for this bath to give reproducible results. The internal stress is slightly higher than in deposits from Watts solutions. The disadvantages of the hard-nickel bath are its tendency to form nodules on edges and the low annealing temperature (230°C) of its deposits (Di Bari, 2000).

*All-Chloride bath* is an alternative process where high current densities are required. These solutions are also much more corrosive than Watts solutions and therefore equipment must be carefully selected. Deposits are fine-grained and generally harder than Watts nickel coatings (Rose & Whittington, 2002).

The major use for *all-sulphate bath* is in applications involving the use of insoluble anodes (e.g. in the internal plating of pipes and fittings). The absence of chlorides eliminates the problem of toxic chlorine gas being liberated at the anode. Lead or graphite anodes are commonly employed. It is necessary to replenish the nickel ions and to control the pH through regular additions of nickel carbonate (Rose & Whittington, 2002).

There are at least two formulations for producing black nickel deposits; these incorporate zinc (Zn) and thiocyanate ($CNS^-$) ions. *Black nickel bath* was developed for decorative reasons: color matching and blending. The black nickel deposit has little wear or corrosion resistance and is usually deposited over a layer of nickel deposited from a bright or dull nickel plating solution. Black nickel deposit is still in commercial use, and the deposit is often protected with a clear lacquer coating (Di Bari, 2000).

## 3.3 Nanocomposite Coatings

In a broad sense the word “composite” means “made of two or more different parts.” or “A composite is a combination of two or more different materials that are mixed in an effort to blend the best properties of both.” A composite material consists of an assemblage of two materials of different natures completing and allowing us to obtain a material of which the set of performance characteristics is greater than that of the components taken separately.

Mostly composite material consists of one or more discontinuous phases of distributed in one continuous phase. Hybrid components are that which are with several discontinuous phases of different natures. Discontinuous phase is usually harder and with superior mechanical properties than continuous phase. The continuous phase is called “matrix”. The discontinuous phase is called “reinforcement, or reinforcing material (Berthelot, 2012).

Nanocomposites are composites in which at least one of the phases shows dimensions in the nanometre range (1 nm = $10^{-9}$ m) (Roy, Roy & Roy, 1986). Nanocomposite materials have emerged as suitable alternatives to overcome limitations of microcomposites and monolithics, while posing preparation challenges related to the control of elemental composition and stoichiometry in the nanocluster phase (Camargo, Satyanarayana & Wypych, 2009).

Nanocomposite materials can be classified, according to their matrix materials, in three different categories as shown in Table 3.3.

Table 3.3 Different types of nanocomposites (Camargo et al., 2009)

| Class | Examples |
|---|---|
| Metal | Fe-Cr/$Al_2O_3$, Ni/$Al_2O_3$, Co/Cr, Fe/MgO, Al/CNT, Mg/CNT |
| Ceramic | $Al_2O_3$/$SiO_2$, $SiO_2$/Ni, $Al_2O_3$/$TiO_2$, $Al_2O_3$/SiC, $Al_2O_3$/CNT |
| Polymer | Thermoplastic/thermoset polymer/layered silicates, polyester/$TiO_2$, polymer/CNT |

### *3.3.1 Metal Matrix Nanocomposites*

Metal matrix composites (MMCs) reinforced with nano-particles, also called Metal Matrix nano-Composites (MMnCs), are being investigated worldwide in recent years, owing to their promising properties suitable for a large number of functional and structural applications. The reduced size of the reinforcement phase down to the nano-scale is such that interaction of particles with dislocations becomes of significant importance and, when added to other strengthening effects typically found in conventional MMCs, results in a remarkable improvement of mechanical properties (Casati & Vedani, 2014).

### *3.3.2 Ceramic Matrix Nanocomposites*

Ceramics stand, in principle at least, to benefit from the incorporation of nanomaterials, most notably CNTs. While strong and hard, most ceramics have low fracture toughness and are therefore brittle. Despite the availabilityof ceramics toughened with carbon and silicon carbide (SiC) fibres (ceramic matrix composites), prevailing research aims to develop CNT-based ceramic nanocomposites with improved properties. Nanotube reinforcements promise to increase the material's fracture toughness by absorbing energy through their highly elastic behaviour during deformation.

### *3.3.3 Polymer Matrix Nanocomposites*

Polymer composites are manufactured commercially for many diverse applications such as sporting goods, aerospace components, automobiles, etc (Hussain, Hojjati, Okamoto & Gorga, 2006). Generally, polymer nanocomposites are the result of the combination of polymers and inorganic/organic fillers at the nanometer scale (Gorrasi et al., 2008). The interaction between nanostructures and polymer matrix is the basis for enhanced mechanical and functional properties of the nanocomposites as compared to conventional microcomposites (Armentano, Dottori, Fortunati, Mattioli & Kenny,

2010). In addition, many polymer nanocomposites can be fabricated and processed in ways similar to that of conventional polymer composites, making them particularly attractive from a manufacturing point of view (Hussain et al., 2006).

### 3.4 Ni Matrix Nanocomposite Coatings

Over the past few years, metal matrix composite coatings, especially nickel matrix composite coatings containing nano-particles which exhibit excellent properties, such as higher wear and corrosion resistance, higher hardness, and more excellent self lubricating in comparison with single metal coating, have been more widely studied. The coating properties improved with decreasing of codeposited particles size. Corrosion resistance can be affected by microstructure, such as grain size, surface morphology and texture, which is closely related to the electrodeposition parameters, such as current density, pH, electrolyte temperature and particle concentration of the plating bath (Rusu, Cojocaru, Magagnin, Gheorghies & Cârâc, 2010). Metal matrix composite coating containing alumina ($Al_2O_3$) and titania ($TiO_2$) particles has been widely used in industry. Although Ni-$TiO_2$ composites have been reported to be advantageous for high temperature (Lin, Lee, Chang & Chang, 2006), interesting photoelectrochemical and photocatalytical behavior application (Feng et al., 2008) relatively little research effort has been dedicated to the electrodeposition of nickel titania composites (Du, Xu, Dong, Yang & Tu, 2004). The electro co-deposition of Ni with second phase nano-particles such as aluminum oxide, titanium nitride, carbon nanotube (CNTs), diamond, silicon carbide, silicon nitride and zirconium oxide have been studied extensively over the past two decades. A variety of nanosized particles some such investigations with Ni-$Al_2O_3$, Ni-CNTs, Ni-$Si_3N_4$, Ni-diamond, Ni-SiC , Ni-$ZrO_2$, Ni-$TiO_2$ have been reported recently (Rusu et al., 2010). These have the large projected applications for automotive parts, aerospace, printed circuitry and electrical contacts (Hou, Ger, Wang & Ke, 2002).

Rusu and his friends prepared Ni-$TiO_2$ nanocomposite coating by electrochemical deposition. According to their results, $TiO_2$ nanoparticles have a strong influence on the deposit surface morphology. With increasing time for immersion in solution the

corrosion potential decreases, this improvement of corrosion resistance could be due to the fine surface structure of composite coating compared with pure nickel coating as well as to the incorporation of $TiO_2$ nanoparticles into composite coatings (Rusu et al., 2010). Baghery and his friends prepared Ni-$TiO_2$ nanocomposite coatings with various contents of $TiO_2$ nanoparticles by electrodeposition. In this study the microhardness and wear resistance of the nanocomposite coatings increase with increasing of $TiO_2$ nanoparticle content in the coating(Baghery et al., 2010).

Sharma and his colleagues prepared Ni-P-ZnO nanocomposite coating on the surface of mild steel substrate via electroless method. According to results, the electroless Ni-P-ZnO coating exhibits good adherence on the mild steel substrate. For the ‘‘as-coated’’ Ni-P-ZnO coating, the results (micrographs and line spectrum) of chemical composition obtained by FESEM-EDAX suggest that the particles of ZnO are uniformly codeposited in the Ni-P matrix on the substrate surface with some excessive deposition of ZnO particles on the surface of the coating (Sharma, Sharma, Sharma & Agarwala, 2016).

Hassan and Abdel Hamid prepared Ni-$Cr_2O_3$ nanocomposite coating on carbon electrode via electrodeposition technique from nickel Watts bath in presence of $Cr_2O_3$ nanoparticles. From the results, the co-deposition of nano-sized $Cr_2O_3$ particles in a metal deposit modified the surface morphology of nickel matrix and reduced the size of Ni grains (Hassan & Hamid, 2011). Liu and Xu focused on to investigate the role of $Cr_2O_3$ nanoparticles on the erosion-corrosion behavior of composite alloying layer. According to their research, Ni/$Cr_2O_3$ composite alloying layer with compact, uniform structure and good bonding with substrate is formed on the surface of 316L stainless steel, and $Cr_2O_3$ nanoparticles do not decompose or react with their surrounding matrix under alloying temperature (1000°C) condition. The results of erosion-corrosion tests indicate that the erosion-corrosion resistance of Ni/$Cr_2O_3$ composite alloying layer is the highest in investigated materials, and the dynamic action of the slurry does not severely decrease the corrosion resistance and protective efficiency of Ni/$Cr_2O_3$ composite alloying layer (Liu & Xu, 2011).

## 3.5 Production Methods of Nanocomposite Coatings

The most common techniques for the processing of nanocomposites are (Baker, Shah & Hasanain, 2004) spray pyrolysis; liquid metal infiltration; rapid solidification; vapour techniques (PVD, CVD); electrodeposition and chemical methods, which include colloidal and sol-gel processes (Camargo et al., 2009).

Wu and his colleagues prepared Ni-$TiO_2$ nanocomposite by a sol-gel process. According their study, the phase structure and grain size of the nanocomposites could be manipulated by altering the heat-treatment conditions. The nanocomposites possess a mesoporous structure, and the structural change is related to the nanosized nickel (Y. Wu, X. Wu & Zhang, 2003).

Hou and his colleagues prepared $Cr_2O_3$-IF-$WS_2$ nanocomposite coatings using aerosol-assisted chemical vapor deposition. From the results, hollow onion structure and chemical composition of IF-$WS_2$ nanoparticles are preserved inside the matrix. As compared to pure $Cr_2O_3$ coatings, the nanocomposite coatings have a much rougher surface (Hou, Choy, Brun & Serín, 2013).

Dermenci and his colleagues prepared Ag/ZnO nanocomposite particles via ultrasonic spray pyrolysis method. According their results, with increasing temperature, sintering and agglomeration mechanism became the most important effect on particle size and morphology (Dermenci, Genc, Ebin, Hanci & Gürmen, 2014).

Faga and his colleagues focused on development and characterization of innovative ceramic coatings for cutting tools with high wear resistance properties at high temperatures. AlSiTiN nanocomposite coatings were developed via Arc Cathodic PVD method. According to their study, formation of an oxidised protective layer of alumina and alumina–silica was proposed for AlTiN and nanocomposites coatings, respectively, inducing an increase of wear resistance with respect to AlCrN coating, for which similar phenomena were not evident (Faga et al., 2007).

### *3.5.1 Electrodeposition Method*

Electrodeposition of metals or its oxides is one of oldest themes in electrochemical science (Conway, 1965). The first studies on this topic are dated from early nineteenth century, using galvanic cells as a power source (Parsons, 1959) and electrodeposition remains a much studied topic till today. Themes as supercapacitors or electrochemical cells devices have raised considerable attention (Wang et al., 2013). In this case, the electrodeposition technique is of great interest due to their unique principles and flexibility in the control of the structure and morphology of the oxide electrodes (Garcia, Lins & Matencio, 2013). Electrodeposition which offers several advantages when compared with other techniques including precise control, low energy requirements, uniform deposition, low cost in production of large area samples, good reproducibility, versatility, capability to coat complex component geometries, high production rate and reduction of waste (Ahmad & Mohamed, 2014; Saha & Khan, 2010).

The electrodeposition process essentially involves passing an electric current between two electrodes immersed in an electrolyte. The positively charged electrode is known as the anode while the negatively charged electrode is the cathode. The electrolyte contains electrically charged particles or ions. When an electrical potential or voltage is applied between the electrodes these ions migrate towards the electrode with the opposite charge positively charged ions to the cathode and negatively charged ions to the anode. This results in the transfer of electrons that is a current flow, between the electrodes thus completing the electrical circuit. The electrical energy is supplied by a DC power source such as a rectifier. The basic electrical circuit is depicted in Figure 3.1 (Rose & Whittington, 2002).

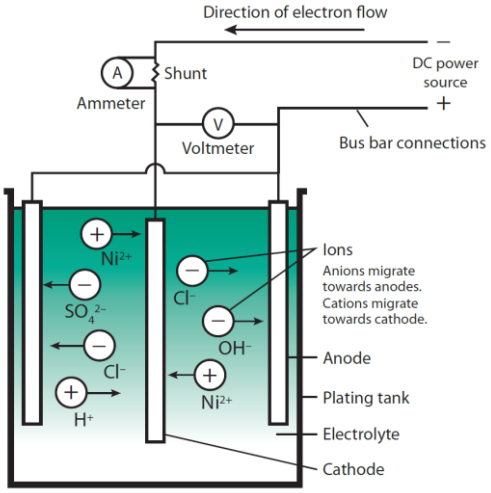


Figure 3.1 Basic electrical circuit for electroplating.

In the early stages of electrodeposition, the limiting step corresponds to electrons transfer from work electrode for metallic ions in solution. In this case the relation between the current and the overpotential for electrodeposition is given by Eq. 3.1 (Conway, 1965). In this equation, F is Faraday's constant, k is a constant, C is the concentration of metal ions in solution, α corresponds to a coefficient of symmetry (near 0.5), η corresponds to overpotential, R is the ideal gas constant and T the absolute temperature, in Kelvin. There is an exponential dependence between the current and applied overpotential. Obviously that, with increasing of overpotential, the ionic current that electrolyte can supply is limited by the other processes as such material transport or electrical conductivity (Conway, 1952). Through Coulomb's law, we obtain the relation of thickness with the charge density (d = MMq/nFρ). Where, MM corresponds to the molecular weight, q is the charge density, n corresponds the charge of metal ions and ρ is the density (Garcia et al., 2013).

$$i = -FkCexp(\frac{\alpha F\eta}{RT}) \tag{3.1}$$

In the electrodeposition of $M^{n+}$ ions using the aqueous media (Eq. 3.2) is always observed the hydrogen evolution reaction (HDR) represented by equation 3.3. This results principally in reducing the loading efficiency of electrodeposition (Freitas & Garcia, 2007).

$$M^{n+}_{(aq)} + ne^- \rightarrow M_{(s)} \quad (3.2)$$

$$2H^+_{(aq)} + 2e^- \rightarrow H_{2(g)} \quad (3.3)$$

The electrochemical reactions which occur in nickel electrodeposition process on the cathode could be written generally (Eq. 3.4-3.7) as (Vasilache et al., 2010):

$$Ni^{2+} + 2e^- \rightarrow Ni, \quad (3.4)$$

and the proposed mechanism evolutes after the next steps:

$$Ni^{2+} + H_2O \rightarrow (NiOH)^+ + H^+ \quad (3.5)$$

$$(NiOH)^+ + e^- \rightarrow (NiOH)_{ads} \quad (3.6)$$

$$(NiOH)_{ads} + (NiOH)^+ + 3e^- \rightarrow 2Ni + 2OH. \quad (3.7)$$

Several parameters can influence the electrodeposition process and consequently the microstructure of the composite coating, these parameters include:

*Current density* management is important for two main reasons. Firstly, the current density controls the rate of deposition. Secondly, the current density must be controlled within the correct operating range in order to obtain sound deposits having uniform appearance and free from burning. For optimum productivity, it will be desirable to operate with the maximum surface area of work consistent with the desired current density and the available current. In practice, the size, shape or weight of the work may limit the surface area that can be loaded. In such cases, the current may need to be reduced to achieve the desired current density. The control of current density is particularly critical where work is being plated to a specified thickness and where the equipment operates on a fixed time cycle (Rose & Whittington, 2002).

Changes in *temperature* can affect the performance of nickel plating and other process solutions. Specifically, temperature can influence the brightness range, throwing power, ductility, hardness, internal stress and burning characteristics (Rose & Whittington, 2002).

*pH* is a measure of the hydrogen ion concentration, or more simply the acidity, of a solution. In the case of nickel solutions the pH has an important influence on bath performance. The pH can affect the bright plating range, cathode efficiency, effects of impurities, throwing power, stress, as well as the physical properties of the deposit. Despite the use of boric acid as a buffer, the pH continually changes. Under normal operating conditions the pH tends to rise and this must be counteracted by the addition of dilute sulphuric or hydrochloric acid. If the pH falls this will indicate either drag-in of an acid (e.g. from an acid dip), abnormal anode behavior, or the use of insoluble anodes. The pH can be increased by stirring in a slurry of nickel carbonate or, less preferably, sodium hydroxide (Rose & Whittington, 2002).

# CHAPTER FOUR
# EXPERIMENTAL STUDIES

This study includes synthesis and characterizations of $TiO_2$, ZnO and $Cr_2O_3$ nanoparticles and Ni based nanocomposite coatings. Nanoparticles were synthesized via sol-gel method. Nanocomposite coatings containing nanoparticles with different sizes and concentration in a nickel matrix have been prepared by means of electrodeposition process from Watts bath.

## 4.1 Synthesis of Nanoparticles

### *4.1.1 Synthesis of $TiO_2$ Nanoparticles*

$TiO_2$ nanoparticles which used in these studies were obtained by the sol-gel method. $TiO_2$ nanoparticles were synthesized by using titanium tetraisopropoxide (TTIP) as the Ti-precursor, glacial acetic acid and deionised water. Two different types of solutions were prepared in order to produce $TiO_2$ nanoparticles. In first method, titanium (IV) isopropoxide was dissolved in glacial acetic acid, it acts as a catalyst to prevent titanium isopropoxide from the nucleophilic's attack by the water (Doeuff, Henry, Sanchez & Livage, 1987) and deionised water with the molar ratio of 1:10:200. The solution was stirred for two hours on a magnetic stirrer. On the other hand, freshly water-soluble egg white proteins were homogenized in water by stirring on a magnetic stirrer. Then, the egg white solution was added into the precursor solution. Final solution was dried at 80°C overnight. Finally, the dried gel was grinded in mortar and calcined in a muffle furnace at 500°C for 5 hours. $TiO_2$ nanoparticles which obtained by the first method were called as $TiO_2$-A. The flow chart of the solution preparation ($TiO_2$-A) is illustrated in Figure 4.1.

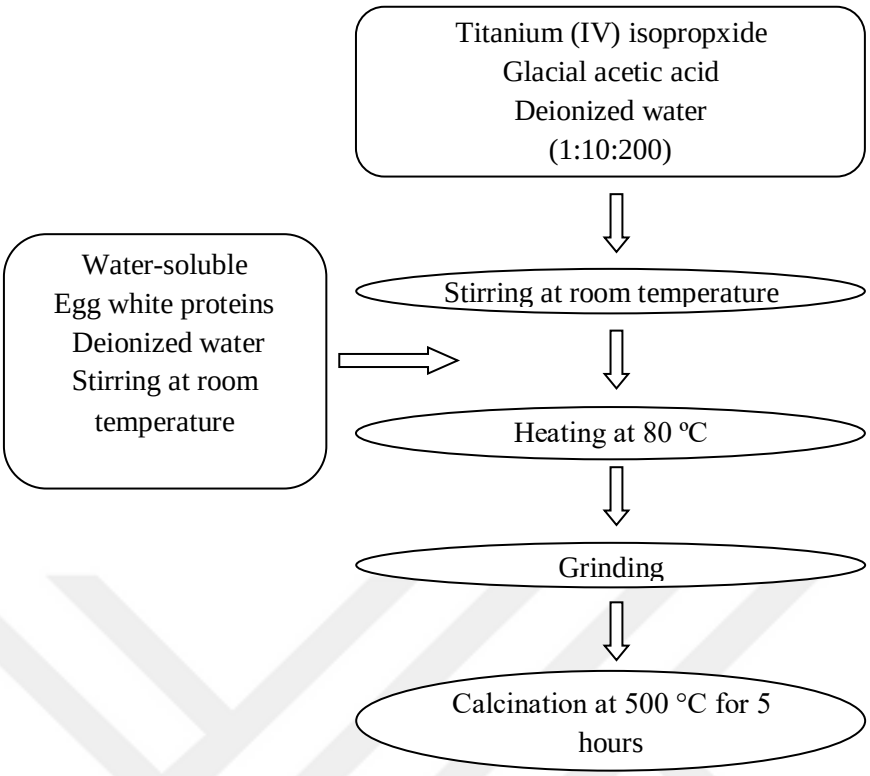


Figure 4.1 Schematic illustration of sol $TiO_2$-A preparation.

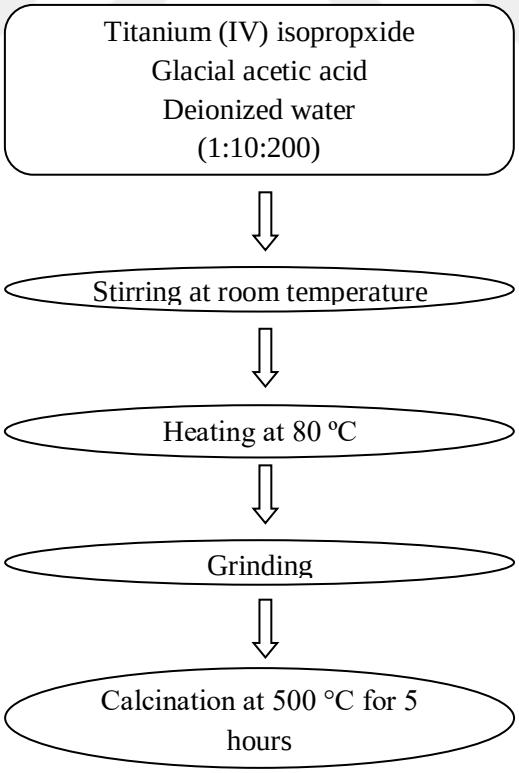


Figure 4.2 Schematic illustration of sol $TiO_2$-B preparation.

In the second method, the precursor solution was prepared by same method as mentioned above. Then, the solution was stirred and and dried at about 80°C. The dried gel was grinded and calcined in a muffle furnace at 500°C for 5 hours (Bagheri et al., 2012).$TiO_2$ nanoparticles which synthesized via the second method were called as $TiO_2$-B. The flow chart of the solution preparation ($TiO_2$-B) is illustrated in Figure 4.2.

### *4.1.2 Synthesis of ZnO Nanoparticles*

ZnO nanoparticles were synthesized by sol-gel method. Two different aging time was used in the process. Figure 4.3 shows that flowchart of Zn-1 and Zn-2 nanoparticles.

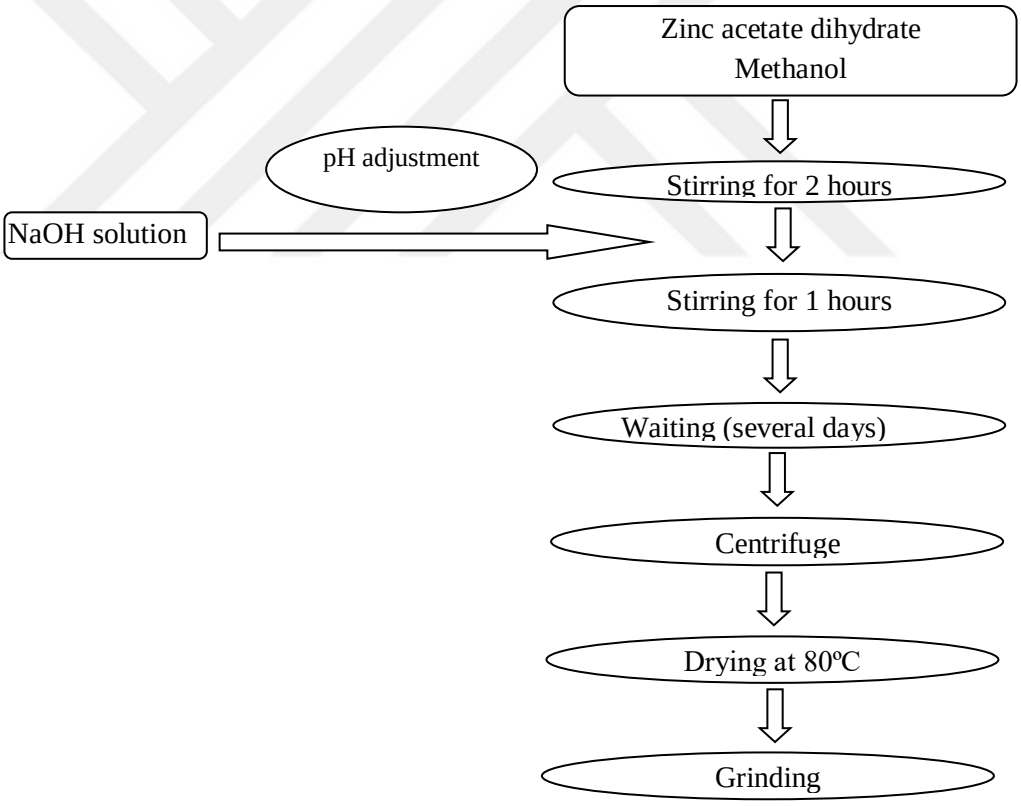


Figure 4.3 Schematic illustration of ZnO nanoparticles preparation by sol-gel technique.

The ZnO sols were prepared by adding 0.05M zinc acetate dehydrate to methanol at room temperature. The solution was stirred for 2 h using a magnetic stirrer until a

clear solution without turbidity was obtained. The solution turned into a white slurry solution after titration with 1.0 M NaOH. The result pH of sol was found be 11. Then the solution was stirred for another 1h. The resulting solutions were left alone for several days (Zn-1), (Zn-2) to allow the sol-gel process to finish. After aging process, the sols were centrifuged at 3000 rpm for 30 min to complete gelation and hydrolysis. Nano ZnO precipitates was first treated in 80°C oven to remove the remaining water. Finally, ZnO nanoparticles were grinded with mortar to be shaped into powder (Alias, Ismail & Mohamad, 2010).

### *4.1.3 Synthesis of $Cr_2O_3$ Nanoparticles*

$Cr_2O_3$ nanoparticles were synthesized via sol-gel method. Two different molarities were used in process. The flowchart of $Cr_2O_3$ nanoparticles are shown in Figure 4.4.

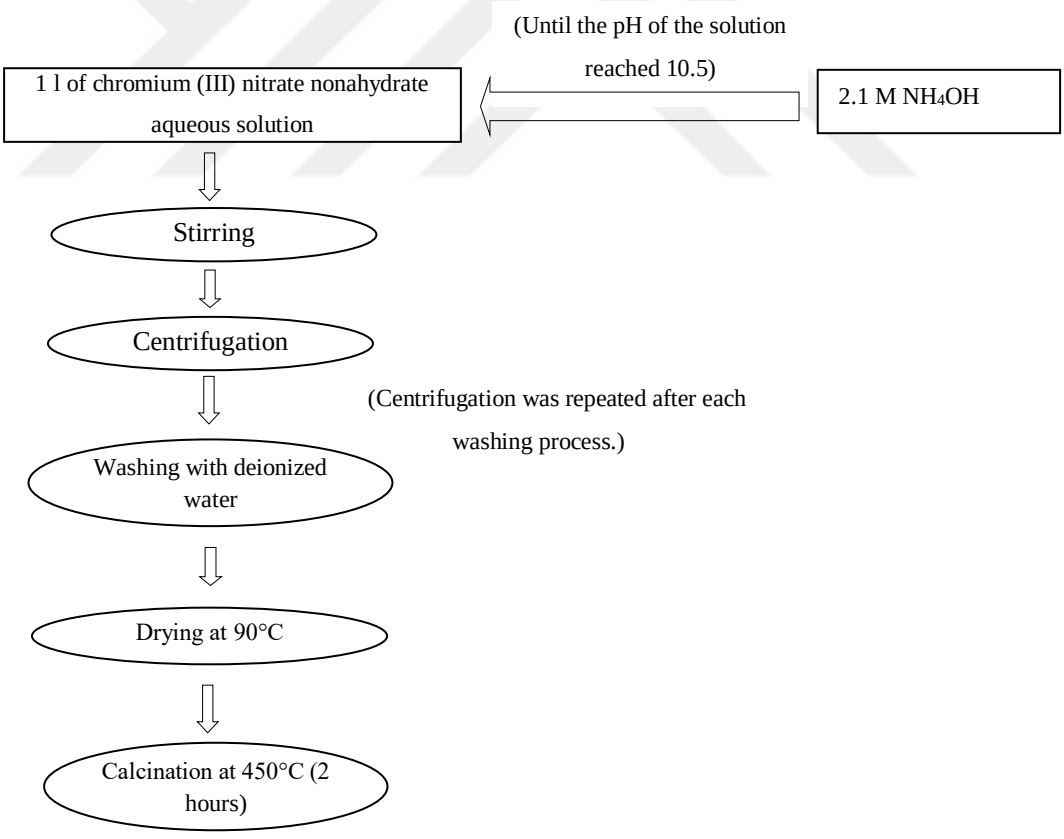


Figure 4.4 The flowchart of $Cr_2O_3$ nanoparticles.

Chromic hydroxide hydrate was prepared by adding $NH_4OH$ aqueous solution into 0.9M (Cr-1) or 1M (Cr-2) chromium (III) nitrate nonahydrate aqueous solution until the pH of the solution reached 10.5 under vigorous stirring with mechanical stirrer. After 90 min, centrifugal force was applied to make chromium hydroxide hydrate to be separated. Separated chromic hydroxide hydrate was washed with deionized water three times. During the washing process centrifugal force was applied to the samples to shorten the sedimentation time. Finally, chromic hydroxide hydrate was converted into chromic oxide by calcination at 450°C for 2 h (Kim, Shin, Lee & Oh, 2004).

## 4.2 Production of Pure Ni and Ni Based Nanocomposite Coatings

### *4.2.1 Preparation of Substrate*

Steel with dimensions of 100mmx25mm was used as substrate. Firstly, the substrates were polished with SiC paper (1200 grit). Then the substrates were etched in etching solution for 1 min. Table 4.1 shows ingredients of etching solution. Finally the substrates were washed with deionized water and rinsed ethanol.

Table 4.1 The ingredients of etching solution

| **Chemicals** | **Amount (ml)** |
|---|---|
| Deionized water | 80 |
| Nitric acid (%65) ($HNO_3$) | 15 |
| Hydrofluoric acid (HF) | 5 |

### *4.2.2 Preparation of Pure Ni and Ni Matrix Nanocomposite Coatings*

Pure Ni and Ni based nanocomposite coatings were deposited on steel substrates by electrodeposition process. Watts bath was used as an electroplating bath. Table 4.2 shows that the composition of Watts bath. $TiO_2$, ZnO and $Cr_2O_3$ nanoparticles were used for preparation of nanocomposite coatings. These nanoparticles were added to the deposition bath at different concentration and particle size in Watts bath. Before electrodeposition process, the Watts baths had been stirred for 24 hours to keep the particles dispersed and prevent sedimentation in the electrolyte suspension. Also,

during the electrodeposition process the bath was stirred by a magnetic stirrer. Operating parameters and nomenclature of the coatings were shown in Table 4.3 and 4.4, respectively. Production of Ni and Ni matrix nanocomposite coatings was carried out on steel substrates by electrodeposition method from Watts bath using CHROMA 62050P-100-100 power supply. Nickel plate was used as anode. The experimental setup is illustrated in Figure 4.5.

Figure 4.5 Experimental setup.

Table 4.2 Watts bath composition

| **Chemicals** | **Amount** |
|---|---|
| Nickel Sulfate Hexahydrate ($NiSO_4 \cdot 6H_2O$) | 112.5 g |
| Nickel Chloride Hexahydrate ($NiCl_2 \cdot 6H_2O$) | 15 g |
| Boric acid ($H_3BO_3$) | 15 g |
| Deionized water | 500 ml |

Table 4.3 Deposition conditions

| **Operating Conditions** | |
|---|---|
| Substrate | 304 stainless steel |
| Plating time (min) | 10 |
| Current Density ($A.dm^{-2}$) | 3, 5, 7 |
| Temperature (°C) | 45 |
| Magnetic stirring (rpm) | 200 |

Table 4.4 Nomenclature of the coatings according to the deposition parameters

| | **Nanoparticle** | **Particle size type (nm)** | **Particle Concentration (g/L)** | **Current density ($A.dm^{-2}$)** |
|---|---|---|---|---|
| AE10-3 | - | - | - | 3 |
| AE10-5 | | | | 5 |
| AE10-7 | | | | 7 |
| E50-1T-3 | $TiO_2$ | <50 | 1 | 3 |
| E50-1T-5 | | | | 5 |
| E50-1T-7 | | | | 7 |
| E50-3T-3 | | | 3 | 3 |
| E50-3T-5 | | | | 5 |
| E50-3T-7 | | | | 7 |
| E80-1T-3 | | >50 | 1 | 3 |
| E80-1T-5 | | | | 5 |
| E80-1T-7 | | | | 7 |
| E50-1Z-3 | ZnO | <50 | 1 | 3 |
| E50-1Z-5 | | | | 5 |
| E50-1Z-7 | | | | 7 |
| E80-1Z-3 | | >50 | 1 | 3 |
| E80-1Z-5 | | | | 5 |
| E80-1Z-7 | | | | 7 |
| E50-1C-3 | $Cr_2O_3$ | <50 | 1 | 3 |
| E50-1C-5 | | | | 5 |
| E50-1C-7 | | | | 7 |
| E50-3C-3 | | | 3 | 3 |
| E50-3C-5 | | | | 5 |
| E50-3C-7 | | | | 7 |
| E80-1C-3 | | >50 | 1 | 3 |
| E80-1C-5 | | | | 5 |
| E80-1C-7 | | | | 7 |

## 4.3 Characterization of Nanoparticles and Nanocomposite Coatings

### *4.3.1 X-Ray Diffractometer (XRD)*

XRD is a powerful technique used to uniquely identify the crystalline phases present in materials and measure the structural properties (strain state, grain size, epitaxial, phase composition, preferred orientation and defect structure) of these phases. XRD is non-contact and non-destructive. The regular array of atoms in a crystalline material forms a 3D diffraction grating for waves with a wavelength around that of the distance between the atoms. When waves enter a crystal, they are scattered in all directions by the atoms. In certain directions, these waves can interfere destructively. In other directions, constructive interference will occur resulting in peaks in X-ray intensity. The diffraction pattern that results is a map of the reciprocal lattice of the crystal and can be used to determine the structure of the crystal. Bragg's law is the basis for crystal diffraction:

$$n.\lambda=2.d.\sin\theta \qquad (4.1)$$

in which n is an integer known as the order of diffraction, λ is the X-ray wavelength is the spacing between two consecutive scattering planes and θ is the angle between the atomic planes and the incident (and diffracted) X-ray beam (Ahmed & Jackson, 2014). Figure 4.6 illustrates diffraction of X-rays by planes of atoms.

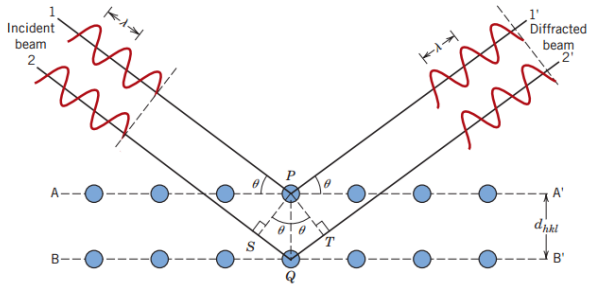


Figure 4.6 Diffraction of x -rays by planes of atoms (A-A ' and B-B ') (Callister & Rethwisch, 2007).

In this study sol-gel synthesized nanoparticles and electrodeposited coatings were analyzed using X-Ray Diffraction (XRD, Rigaku, D/Max-2200/PC) with a grazing

incident angle of 1° at 40 kV and 36 mA using $CuK_\alpha$ radiation with a scanning speed of 4° 2θ/min, from 3° to 90°.

### *4.3.2 Particle Size Distribution (PSD)*

A typical Particle size analyzer system comprises of six main components. First of all a laser is used to provide a light source to illuminate the sample particles within a cell. Most of the laser beam passes straight through the sample, but some is scattered by the particles within the sample. A detector is used to measure the intensity of the scattered light. As a particle scatters light in all directions, it is (in theory), possible to place the detector in any position and it will still detect the scattering. The intensity of the scattered light must be within a specific range for the detector to successfully measure it. If too much light is detected then the detector will become overloaded. To overcome this an "attenuator" is used to reduce the intensity of the laser and hence reduce the intensity of the scattering. The appropriate attenuator position is automatically determined by the Zetasizer during the measurement sequence. The scattering intensity signal for the detector is passed to a digital signal processing board called a correlator. The correlator compares the scattering intensity at successive time intervals to derive the rate at which the intensity is varying. This correlator information is then passed to a computer, where the specialist Zetasizer software will analyse the data and derive size information (Instruments, 2004).

In this study, we used Malvern Zeta Sizer Nano ZS90 device works with laser diffraction principle to determine particle size of $TiO_2$, ZnO and $Cr_2O_3$ particles.

### *4.3.3 Scanning Electron Microscopy and Energy Dispersive Spectrum Analyse*

The Scanning Electron Microscope (SEM) is a versatile electron microscope that images a sample by scanning it with a high-energy beam of electrons in a raster scan pattern. In Typical SEM configuration, electrons are thermoionically emitted from a tungsten or $LaB_6$ cathode filament towards an anode. The electron beam, with a typical

energy ranging from a few KeV to 30 KeV, is focused by successive lenses in a beam with a very fine spot size. When the beam introduces with the surface, different kind of electrons can be detected. The types of signals produced by an SEM include secondary electrons (SE), back-scattered electrons (BSE) and characteristic X-rays. Figure 4.7 illustrates the basic elements of SEM device.

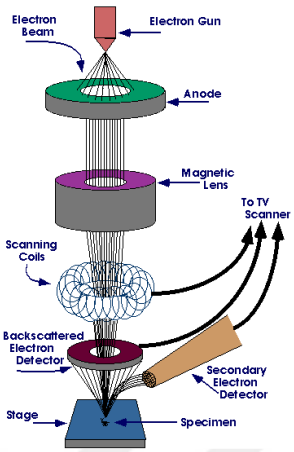


Figure 4.7 Schematic representation of SEM device (Vandaele, 2011).

The energy dispersive spectroscopy (EDS) is often attached to the SEM. The X-rays generated from the interaction between the electron beam and the sample is used to identify and measure quantitatively the elemental composition of the sample. Therefore, SEM/EDS can specify the elemental composition and obtain the morphology of the sample simultaneously.

In this study, the surface and elemental composition of the coatings was examined by using JEOL JSM-6060 Scanning Electron Microscopy with an Energy Dispersive X-ray Spectroscopy (IXRF System EDS) system attachment.

### *4.3.4 Surface Profilometry*

Stylus surface profilometry uses an instrument that amplifies and records the vertical motions of a stylus displaced at a constant speed by the surface to be measured. The Ambios Technology XP-2 surface profilometer used in the present study,

incorporates an optical deflection height measurement mechanism and magneto static force control system which results in a low force (loads as small as 0.05 mg) and low inertia stylus assembly. The stylus tip has a radius of 2μm. Measurement of vertical features ranges from under 10 Å to approximately 400 μm with a vertical resolution of 1.5 Å at 10 μm setting and 15 Å at 100 μm setting, which are specified by the producing company.

### *4.3.5 Nanoindentation*

Hardness is defined as the characteristic ability of a material to resist penetration or abrasion by other bodies. It has been nearly two centuries since the first hardness test was developed by Mohs in 1822. In that time, the state of the art has progressed from using reference materials to rank scratch relative resistance to the application of contact mechanics principles using instrumented, automated systems to probe mechanical properties on the nanometre scale.

Indentation testing is a simple method that consists essentially of touching the material of interest whose mechanical properties such as elastic modulus and hardness. Nanoindentation is simply an indentation test in which the length scale of the penetration is measured in nanometres ($10^{-9}$ m) rather than microns ($10^{-6}$ m) or millimetres ($10^{-3}$ m), the latter being common in conventional hardness tests (Wheeler, 2009).

Nanoindentation hardness tests are generally made with either spherical or pyramidal indenters. Consider a Vickers indenter with opposing faces at a semi-angle of $\theta=68°$ and therefore making an angle $\beta=22°$ with the flat specimen surface. For a particular contact radius a, the radius R of a spherical indenter whose edges are at a tangent to the point of contact with the specimen is given by $\sin \beta = a/R$, which for $\beta=22°$ gives $a/R=0.375$. It is interesting to note that this is precisely the indentation strain at which Brinell hardness tests, using a spherical indenter, are generally performed, and the angle $\theta=68°$ for the Vickers indenter was chosen for this reason (Fischer-Cripps, 2009).

The Berkovich indenter, in Figure 4.8.a, is generally used in small-scale indentation studies and has the advantage that the edges of the pyramid are more easily constructed to meet at a single point, rather than the inevitable line that occurs in the four-sided Vickers pyramid. The face angle of the Berkovich indenter normally used for nanoindentation testing is 65.27°, which gives the same projected area-to-depth ratio as the Vickers indenter. Originally, the Berkovich indenter was constructed with a face angle of 65.03°, which gives the same actual surface area to depth ratio as a Vickers indenter. The tip radius for a typical new Berkovich indenter is on the order of 50–100 nm. This usually increases to about 200 nm with use. The Knoop indenter, in Figure 4.8.b, is a four-sided pyramidal indenter with two different face angles. Measurement of the unequal lengths of the diagonals of the residual impression is very useful for investigating anisotropy of the surface of the specimen. The indenter was originally developed to allow the testing of very hard materials where a longer diagonal line could be more easily measured for shallower depths of residual impression. The cube corner indenter, Figure 4.8.c, is finding increasing popularity in nanoindentation testing. It is similar to the Berkovich indenter but has a semi-angle at the faces of 35.26° (Berkovich, 1951).

Hardness (H) and elastic modulus (E) were calculated from the load-displacement curves according to the procedure outlined by Oliver and Pharr. The Berkovich indenter is used routinely for nanoindentation testing because it is more readily fashioned to a sharper point than the four-sided Vickers geometry, thus ensuring a more precise control over the indentation process. The mean contact pressure is usually determined from a measure of the contact depth of penetration, $h_c$ in such that the projected area of the contact is given by (Oliver & Pharr, 1992);

$$A = 3\sqrt{3}\, h_c^2 tan^2\Theta \tag{4.2}$$

which for $\theta$=65.27°, evaluates to:

$$A = 24.494 h_c^2 \approx 24.5 h_c^2 \tag{4.3}$$

and hence the mean contact pressure, or hardness and elastic modulus, are:

$$H = \frac{P}{24.5h_c^2} \tag{4.4}$$

$$E = \frac{dP}{dh}\frac{1}{2h_c}\frac{1}{\beta}\sqrt{\frac{\pi}{24.5}} \tag{4.5}$$

β = 1.034 for Berkovich indenter

The original Berkovich indenter was designed to have the same ratio of actual surface area to indentation depth as a Vickers indenter and had a face angle of 65.0333°.

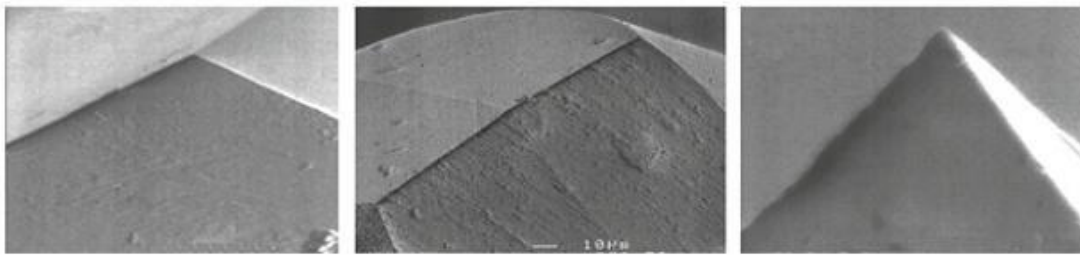

Figure 4.8 SEM images of the tips of (a) Berkovich, (b) Knoop, and (c) cube-corner indenters used for nanoindentation testing. The tip radius of a typical diamond pyramidal indenter is in the order of 100 nm(Fischer-Cripps, 2009).

For the calculation of modulus based on elastic contact theory, there are some differences in view of its indentation deformation. Figure 4.9 depicts the schematic representation of loading versus displacement during nanoindentation. In the figure, S represents the contact stiffness while $h_c$ is the contact depth (Oliver & Pharr, 1992; Ozmetin, Sahin, Ongun & Kuru, 2015).

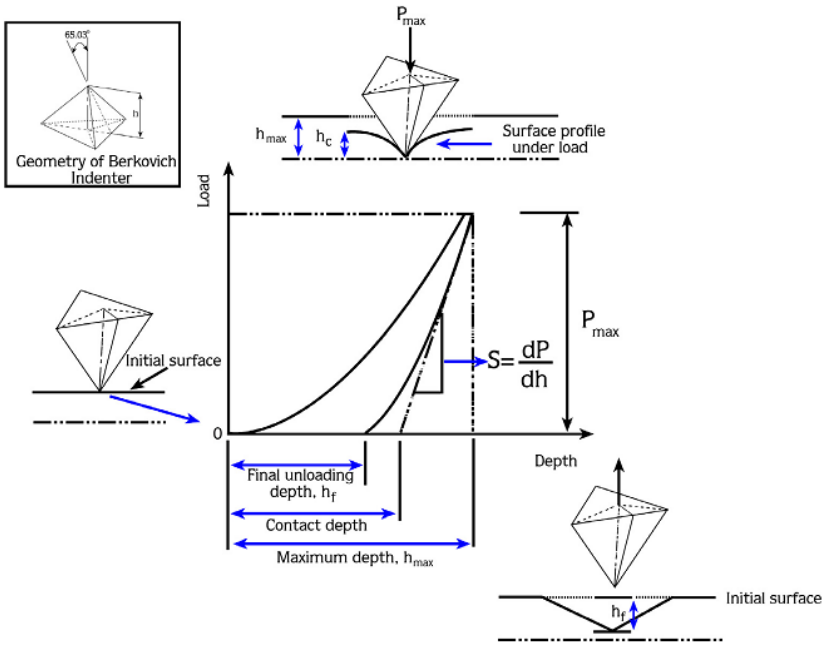


Figure 4.9 Nanoindentation depth–load curve shows the parameters for analysis of the results (Ozmetin et al., 2015).

Nanoindentation measurements of the coatings were performed using a nanoindentation system (IBIS, Fischer-Cripps Laboratories, Australia). We have used a three-side pyramid (Berkovich) diamond indenter. 10 indents were performed on original coating specimens to a force of 150 mN in the present work.

# CHAPTER FIVE
# RESULTS AND DISCUSSION

## 5.1 Sol-Gel Synthesized Nanoparticles

### *5.1.1 Characterization of $TiO_2$ Nanoparticles*

Several synthesis methods of $TiO_2$ nanoparticles have been proposed in literatures including sol-gel, flame synthesis, precipitation and hydrothermal method. The sol–gel process is widely interesting when used in preparation of nano-sized $TiO_2$ because it provides several advantages including high homogeneity and high chemical purity. $TiO_2$ nanoparticles have been modified on crystal phase, particle size, specific surface area, and morphology to provide different products for many applications (Wetchakun, Incessungvorn, Wetchakun & Phanichphant, 2012).

The preparation of $TiO_2$ colloids in the nanometer range can be effectively carried out through the hydrolysis and condensation of titanium alcoxides in aqueous media. In the presence of water, alkoxides hydrolyze and subsequently polymerize to form a three-dimensional oxide network. These reactions can be schematically represented as follows(Mahshid, Ghamsari, Askari, Afshar & Lahuti, 2006):

$$Ti(OR)_4 + 4H_2O \xrightarrow{\text{Hydrolysis}} 2Ti(OH)_4 + 4ROH \quad (5.1)$$

$$Ti(OH)_4 \xrightarrow{\text{Condensation}} TiO_2\ xH_2O + (2- x)H_2O \quad (5.2)$$

The structure of $TiO_2$ nanoparticles which were synthesized via sol-gel method were examined using a X-Ray Diffractometer (XRD). Fig. 5.1 depicts the XRD of $TiO_2$ nanoparticles synthesized from with and without the use of egg white solution. The XRD peaks in the wide angle range of 2θ ascertained that the peaks in 25.367°, 37.909°, 48.158°, 54.051°, 55.204°, 62.867°, 68.976°, 70.479°, 75.303°, and 82.926° can be attributed to the (101), (004), (200), (105), (211), (204), (116), (220), (215) and

(224) crystalline structures of the anatase structure synthesized $TiO_2$ nanoparticles, respectively (Anatase XRD JCPDS Ref. No. 21-1272).

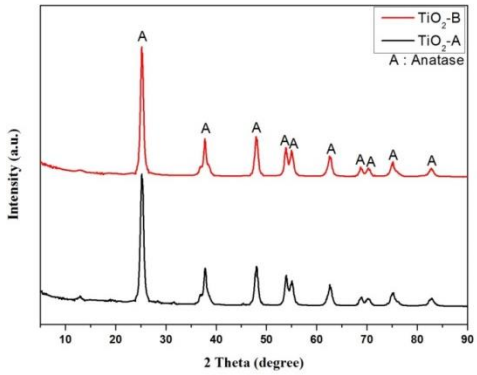


Figure 5.1 X-ray θ-2θ scans of $TiO_2$-A and $TiO_2$-B nanoparticles.

Particle sizes of $TiO_2$ nanoparticles were measured using Malvern Zeta Sizer Nano ZS90. Firstly, 20 mg $TiO_2$ nanoparticles were added into 20 ml deionized water. Then the solution was stirred by ultrasonic probe for 30 min. Figure 5.2 and Table 5.1 show size distribution and particle sizes of $TiO_2$-A and $TiO_2$-B. Particle size measurements indicate that using egg white solution as a matrix decreases the size of particles. The reason for this is water soluble proteins of egg white forms a matrix of entangled polymeric chains, inside the cavities of which can trap small volumes of metal ions. During heat treatment, the dried precursors decompose into nanocrystalline products. The results confirm that egg white solution is an appropriate gelling agent for synthesising $TiO_2$ nanoparticles by using sol-gel method (Bagheri et al., 2012).

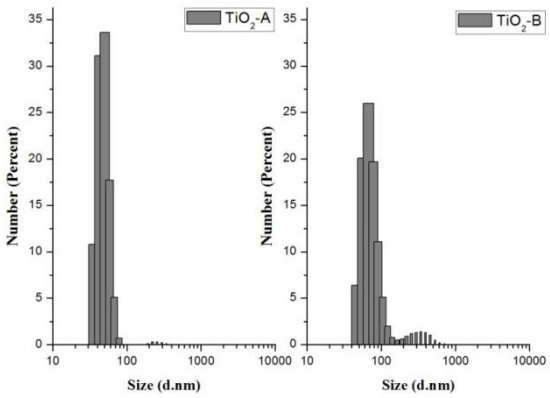


Figure 5.2 Particle size distribution chart of $TiO_2$ nanoparticles.

Table 5.1 Particle sizes of $TiO_2$ nanoparticles

| Sample | Particle Size (nm) |
|---|---|
| $TiO_2$-A | ~49.69 |
| $TiO_2$-B | ~74.39 |

### *5.1.2 Characterization of ZnO Nanoparticles*

Zinc oxide nanoparticles can be prepared by different methods. From these methods, the sol-gel method is more popular because of its cheapness, reliability, repeatability, and simplicity. In addition, the nanoparticles which are produced by this route, show good optical properties. But, this can be achieved only by good control of the size and morphology of the particles. That is, we have to carefully control the sol-gel process and the growth of nuclei must be prevented (Vafaee & Ghamsari, 2007).

The ZnO nanoparticles were synthesized using sol-gel process undergoes four stages; solvation, hydrolysis, polymerization and transformation into ZnO nanoparticles. The zinc acetate dehydrate precursor was first solvated in methanol, and then hydrolyzed which results in a colloidal-gel of zinc hydroxide (Eq. 5.3). This zinc hydroxide splits into $Zn^{2+}$ cation and $OH^-$ anion (Eq. 5.4), followed by polymerization of hydroxyl complex to form ‘‘Zn-O-Zn’’ bridges and finally transformed into ZnO (Eq. 5.5) (Singh, 2012).

$$ZnO(CH_3COO)_2.2H_2O+2NaOH \rightarrow Zn(OH)_2+2CH_3COONa+2H_2O \quad (5.3)$$

$$Zn(OH)_2+2H_2O \rightarrow Zn(OH)_4^{+2} + 2H^{+2} \quad (5.4)$$

$$Zn(OH)_4^{+2} \leftrightarrow ZnO + H_2O + 2OH^- \quad (5.5)$$

The structures of the synthesized ZnO nanoparticles were studied using X-ray diffraction (XRD). Figure 5.3 shows the XRD patterns of ZnO nanoparticles which synthesized different aging time. When Figure 5.3 was examined, it is observed that there is no important difference between XRD patterns of Zn-1 and Zn-2 samples. The diffraction peaks are observed at 2θ value of 31.68, 34.35, 36.16, 47.45, 56.48, 62.74,

67.84 and 68.96° corresponding to the lattice planes (100), (002), (101), (102), (110), (103), (112) and (201) respectively, indicative of hexagonal wurtzite structure of ZnO (JCPDS Ref. No. 36-1451).

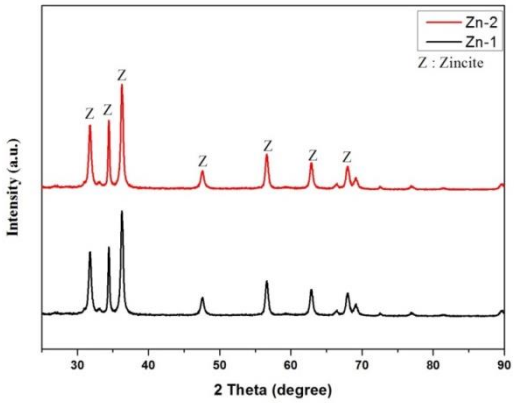


Figure 5.3 X-ray θ-2θ scans of Zn-1 and Zn-2 nanoparticles.

Particle size distribution charts of ZnO nanoparticles which synthesized different aging time are shown in Figure 5.4. It can be clearly observed that the nanoparticles grew as the aging time increased. The results was summarized in Table 5.2.

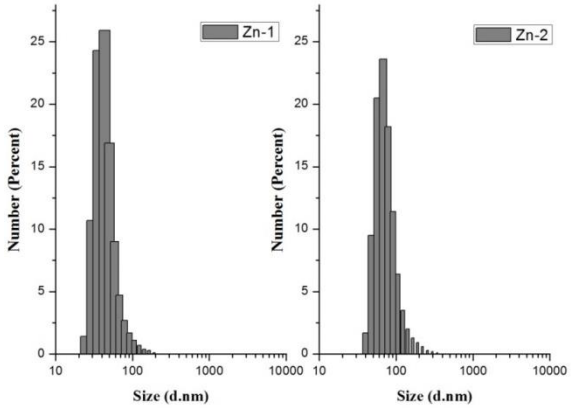


Figure 5.4 Particle size distribution chart of ZnO nanoparticles.

Table 5.2 Particle sizes of ZnO nanoparticles

| Sample | Particle Size (nm) |
|---|---|
| Zn-1 | 48.60 |
| Zn-2 | 79.07 |

### *5.1.3 Characterization of $Cr_2O_3$ Nanoparticles*

Chromium oxide ($Cr_2O_3$) is one of the most important transition metal oxides that are widely used in many industries. They include green pigments, hydrogen storage, gas sensors, coating, wear and corrosion resistance materials, catalysts, digital recording system, magnetic applications, pigments to reflect the infrared radiation from fire and solar energy application (Aghaie-Khafri & Lafdani, 2012). Chromium oxide, ($Cr_2O_3$) particles which exhibit high hardness and a low coefficient of friction and commonly used for wear resistant applications (Srivastava et al., 2010) have been used for incorporation in the present study.

The $Cr_2O_3$ nanoparticles were synthesized via sol-gel process. Firstly, in ethanol solution, nitrate group in $Cr(NO_3)_3 \cdot 9H_2O$ may be replaced by alkoxy group,

$$Cr(NO_3)_3.9H_2O + MetOH \rightarrow Cr(OMet)_3 + HNO_3 + H_2O \quad (5.6)$$

The intermediate $Cr(OEt)_3$ is unstable with the existence of water molecule, and Cr–OEt bond would be hydrolysed to form Cr–OH bond:

$$Cr(OEt)_3 + H_2O \rightarrow Cr(OEt)_x(OH)_{(3-x)} + EtOH \quad (5.7)$$

$$Cr(OEt)_x(OH)_{(3-x)} + xH_2O \rightarrow Cr(OH)_3 + xEtOH \quad (5.8)$$

Then $Cr(OH)_3$ may absorb more water to form $Cr(OH)_3 \cdot 3H_2O$. At elevated temperature, chromium nitrate would directly decompose to $Cr_2O_3$, and chromium hydroxide can form $Cr_2O_3$ via reaction (5.9)(Hou et al., 2013):

$$Cr(OH)_3.3H_2O \rightarrow Cr_2O_3 + H_2O \quad (5.9)$$

To verify the formation of chromic oxide nanoparticles, X-ray diffractometry measurement was performed. The multiple plots of the XRD patterns of particles synthesized at different molarities are shown in Fig. 5.5. The 2θ characteristic peaks

of $Cr_2O_3$ at 24.50, 33.60, 36.21, 41.49, 50.23, 54.86, 65.13 and 73.84° corresponding to the (012), (104), (110), (113), (024), (116), (100) and (119) plane, respectively, of the crystal lattice. These values agree well with those provided by the standard card JCPDS 00-038-1479.

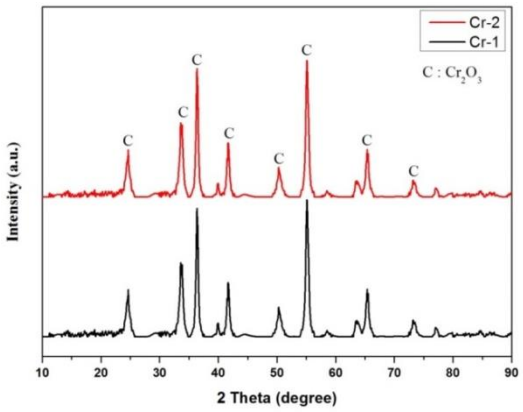


Figure 5.5 X-ray θ-2θ scans of Cr-1 and Cr-2 nanoparticles.

Fig. 5.6 shows that particle size distribution chart of $Cr_2O_3$ nanoparticles. As it can be seen in Fig. 5.6, the particle size of $Cr_2O_3$ nanoparticles increased when the molar ratio of the chromium (III) nitrate nonahydrate was increased. The particle sizes of $Cr_2O_3$ nanoparticle samples prepared under different experimental conditions is presented in Table 5.3.

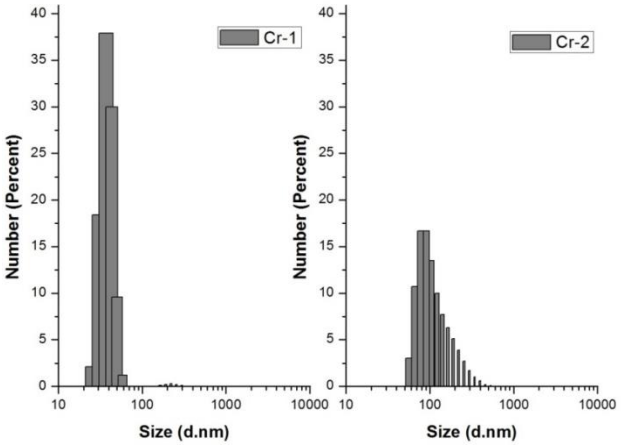


Figure 5.6 Particle size distribution chart of $Cr_2O_3$ nanoparticles.

Table 5.3 Particle sizes of $Cr_2O_3$ nanoparticles

| Sample | Particle Size (nm) |
|---|---|
| Cr-1 | 48.15 |
| Cr-2 | 123 |

## 5.2 Characterization of Pure Ni Coatings

Fig. 5.7 shows XRD pattern of nickel coating without addition of ceramic particles which synthesized different current densities. All XRD patterns show typical peaks of nickel at 44.48, 51.83 and 76.35° corresponding to (111), (200) and (220) crystallographic planes of nickel, respectively (JCPDS Ref. No. 70-1849) (Bakhit & Akbari, 2013).

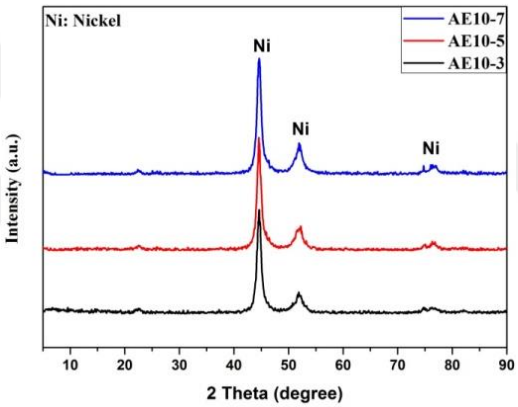


Figure 5.7 X-ray θ-2θ scans of Ni coatings at 3, 5 and 7 A $dm^{-2}$.

## 5.3 Characterization of Electrodeposited Ni-$TiO_2$ Nanocomposite Coatings

The XRD diagrams of nanocomposite coatings prepared at different current densities and different concentrations are illustrated in Fig. 5.8. It should be noticed that the peak at 25.3° can be assigned to (100) plane of anatase and cannot be clearly distinguished due to relatively high intensity of nickel diffraction peaks(Lajevardi & Shahrabi, 2010). All of the XRD patterns show typical peaks corresponding to (111), (200) and (220) crystalline planes of nickel (JCPDS Ref. No. 70-1849).

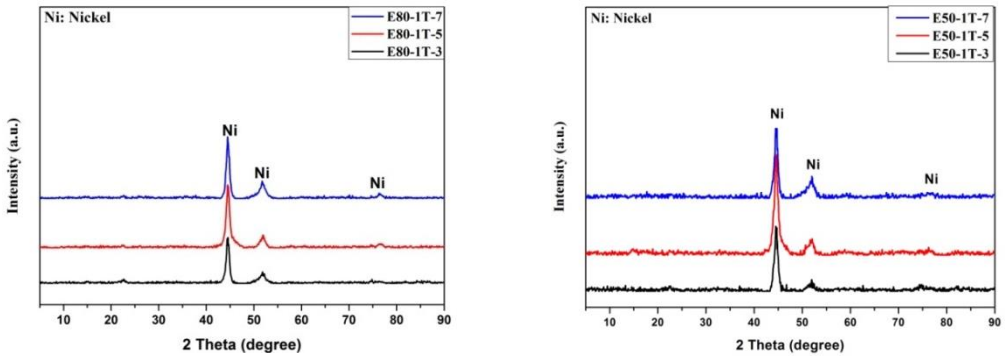


(a)




(b)

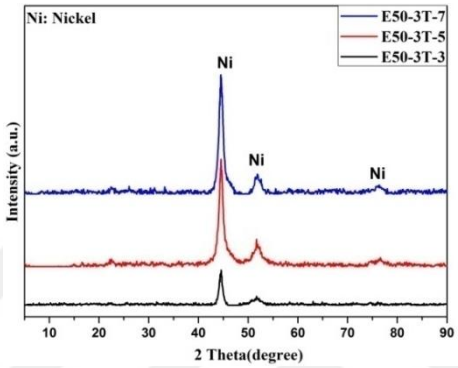


(c)

Figure 5.8 X-ray θ-2θ scans of Ni-$TiO_2$ nanocomposite coatings with $TiO_2$ nanoparticles (a) 80 nm sized and 1 gr/lt concentration, (b) 50 nm sized and 1 gr/lt concentration and (c) 50 nm sized and 3 gr/lt concentration electrodeposited at 3, 5 and 7 A $dm^{-2}$ current densities.

The surface morphologies of Ni-$TiO_2$ nanocomposite coatings which synthesized different operating conditions are shown in Fig. 5.9. The Ni-$TiO_2$ nanocomposite coating shows particulate-like structure in appearance compare to that of pure Ni coating. Additionally, it is evident from the surface morphologies that as the wt.% of $TiO_2$ nanoparticles increases, the surface which shows particulate-like appears bigger (Khalil, Eldin, Hassan, El-Sayed & Hamid, 2015). Baghery and his colleagues prepared Ni-$TiO_2$ nanocomposite coatings with various contents of $TiO_2$ nanoparticles via electrodeposition. According to their study, The pure Ni coating demonstrated a rather regular surface. The Ni-$TiO_2$ nanocomposite coating shows smother surface, more uniform and compact in appearance compare to that of pure Ni coating, which indicates that the codeposited $TiO_2$ nanoparticles were uniformly distributed in the Ni matrix of nanocomposite coating (Baghery et al., 2010). Thiemig and Bund prepared nanocomposites containing titania nanoparticles in a nickel matrix. From their results,

The surface morphology as well as the microstructure of the nickel matrix is significantly altered due to the addition of titania particles to the plating bath. The nanosized particles inhibit the nickel growth and thus lead to a smaller nickel crystallite size combined with a loss of texture (Thiemig & Bund, 2008).

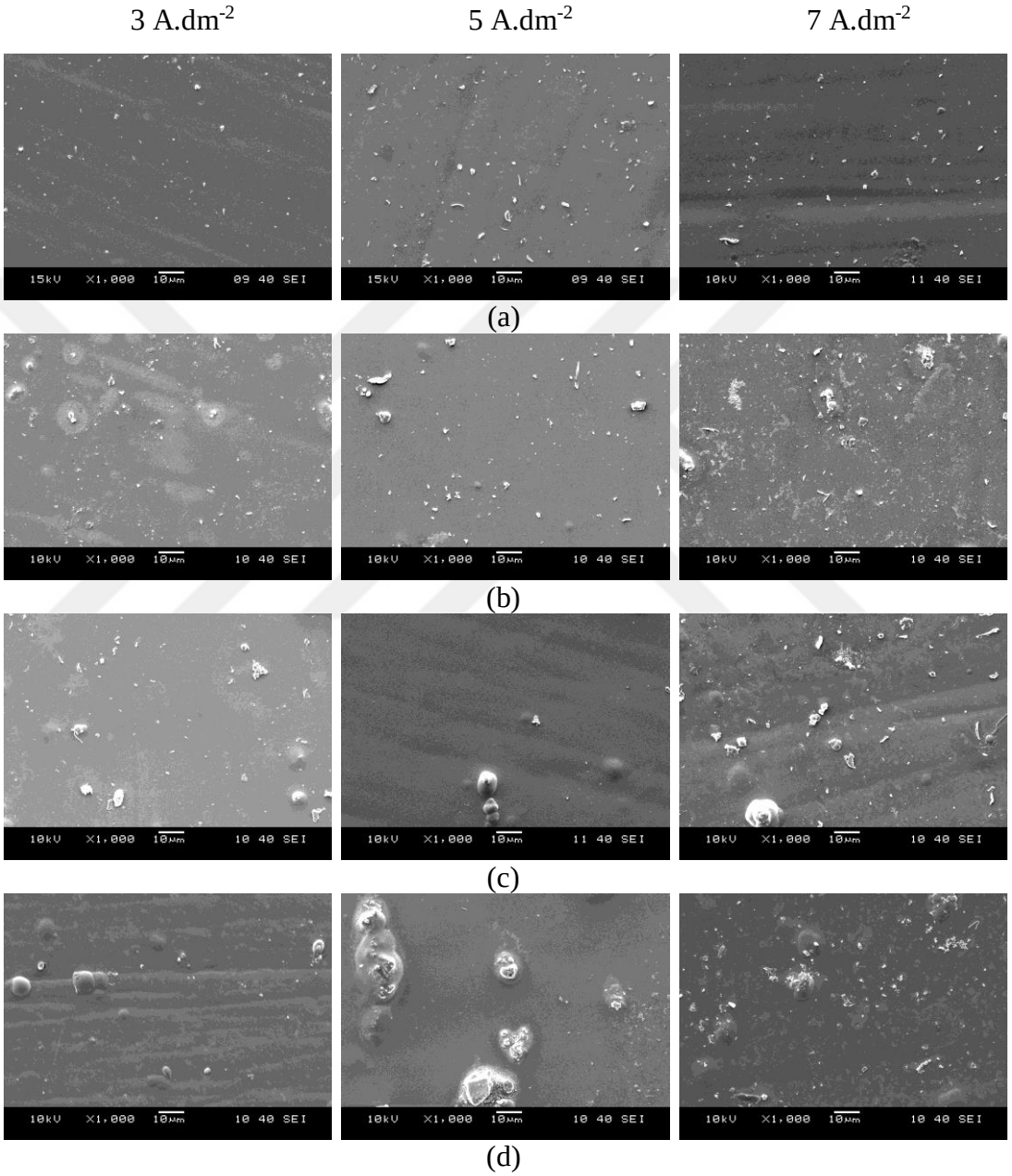


Figure 5.9 Surface morphologies of (a) pure nickel and Ni-$TiO_2$ nanocomposite coatings with $TiO_2$ nanoparticles (b) 80 nm sized and 1 gr/lt concentration, (c) 50 nm sized and 1 gr/lt concentration and (d) 50 nm sized and 3 gr/lt concentration electrodeposited at 3, 5 and 7 A $dm^{-2}$ current densities.

In other study, Parida and his colleagues prepared ultrafine $TiO_2$ dispersed nickel composite coatings by direct current deposition process on steel substrate from Watts bath. According to their research, with increase in $TiO_2$ amount in the coating surface roughness increases marginally(Parida, Chaira, Chopkar & Basu, 2011).

Figure 5.10 shows the results of the SEM-EDS mapping analysis study to determine the distribution of $TiO_2$ nanoparticles by nanocomposite coatings. The mapping images of only E50-3T-5 were given to represent all of the coatings. According the SEM-EDS mapping analysis, the distribution of Ti particles is uniformly homogenous in all the coatings.

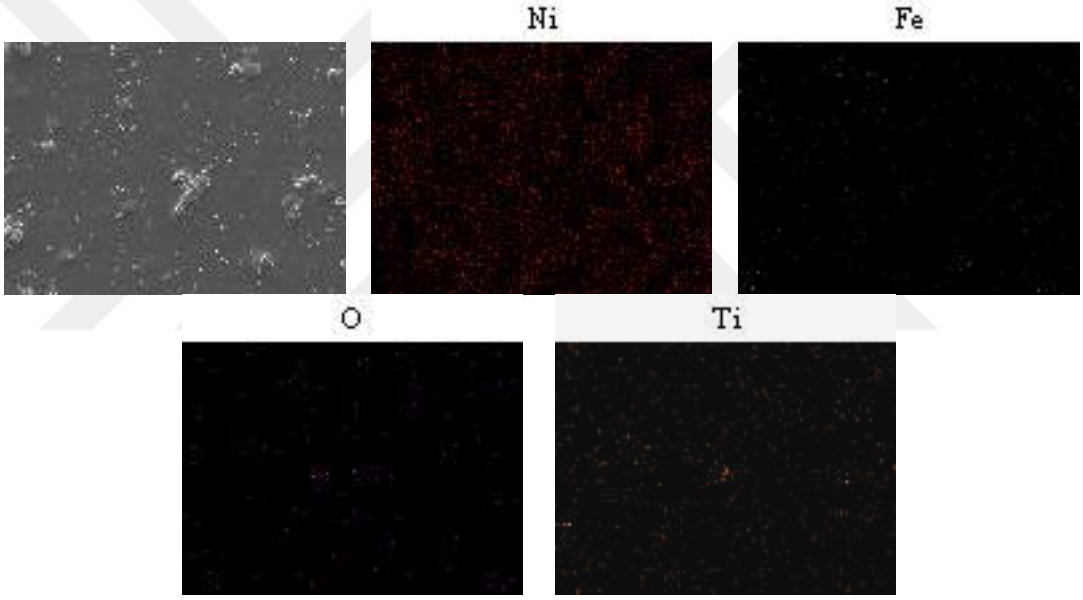


Figure 5.10 Mapping images of Ni-$TiO_2$ nanocomposite coatings with 50 nm sized and 3 gr/lt concentration $TiO_2$ nanoparticles.

## 5.4 Characterization of Electrodeposited Ni-ZnO Nanocomposite Coatings

The crystal structure of the Ni-ZnO nanocomposite coatings was determined by X-ray diffraction. Fig. 5.11 shows the XRD patterns of Ni-ZnO nanocomposite coatings synthesized at different current densities and ZnO particle size. The 2θ characteristic peaks of nickel at 44.48°, 51.83° and 76.35° corresponding to (111), (200) and (220) planes of the crystal lattice, respectively (Bakhit & Akbari, 2013; Parida et al., 2011).

All of the recorded peaks; in the XRD patterns, belong to the Ni matrix of the nanocomposite coatings and no peak was detected from the ZnO phase. The absence of ZnO peaks in the XRD patterns is related to the low amount and small size of ZnO nanoparticles (Bakhit & Akbari, 2013).

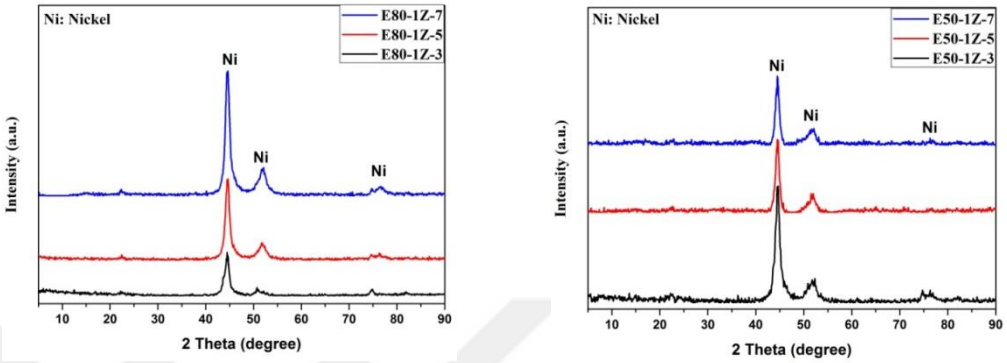


(a) (b)

Figure 5.11 X-ray θ-2θ scans of Ni-ZnO nanocomposite coatings with ZnO nanoparticles (a) 80 nm sized and 1 gr/lt concentration, (b) 50 nm sized and 1 gr/lt concentration electrodeposited at 3, 5 and 7 A $dm^{-2}$ current densities.

The morphology of all the Ni-ZnO nanocomposite coatings was investigated by SEM and mapping analyses. Fig. 5.12 illustrates the SEM images showing surface morphologies of the Ni-ZnO nanocomposite coatings deposited at different current densities and ZnO particle size. The Ni-ZnO nanocomposite coating shows smother surface, more uniform and compact in appearance compare to that of pure Ni coating, which indicates that the codeposited ZnO nanoparticles were uniformly distributed in the Ni matrix of nanocomposite coating (Baghery et al., 2010).

Fig. 5.13 shows the mapping of the elements on the surface of Ni-ZnO nanocomposite coatings. From Fig. 5.13 we can see that ZnO nanoparticles show uniform distribution in all the samples.

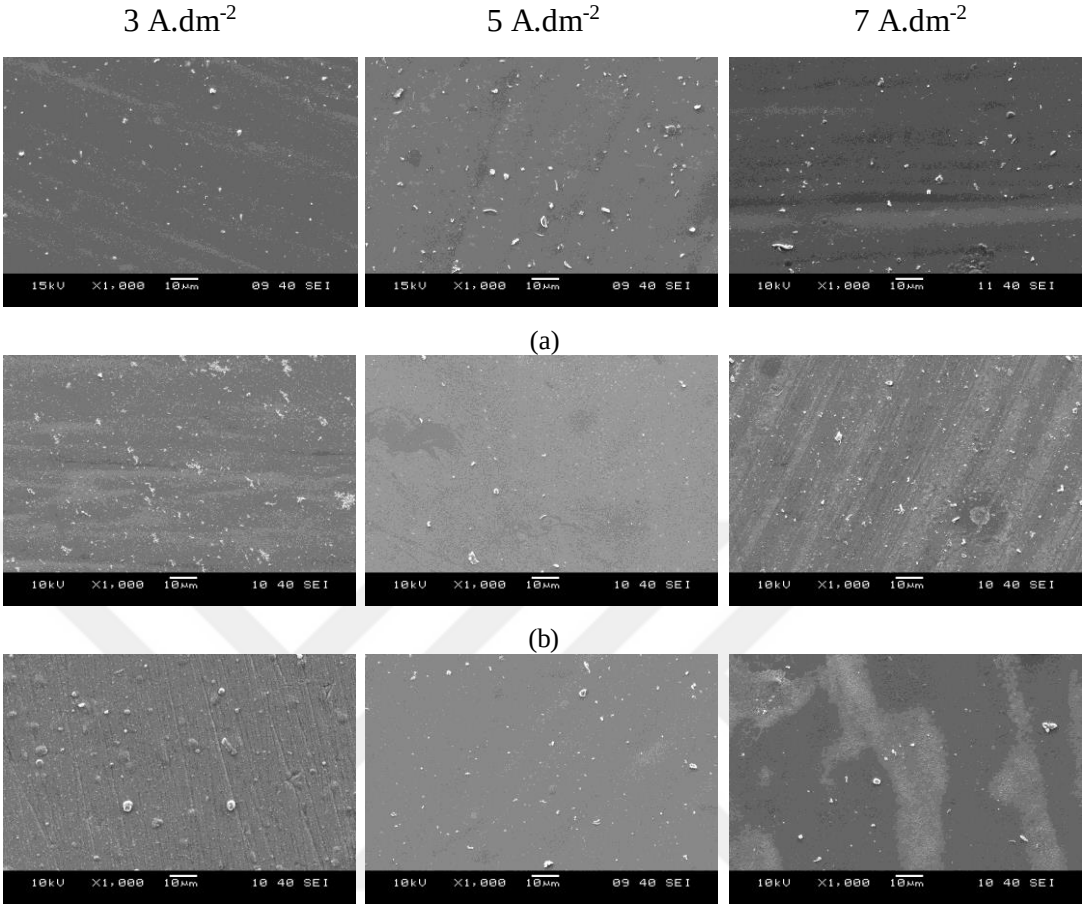


Figure 5.12 Surface morphologies of (a) pure nickel and Ni-ZnO nanocomposite coatings with ZnO nanoparticles (b) 80 nm sized and 1 gr/lt concentration, (c) 50 nm sized and 1 gr/lt concentration electrodeposited at 3, 5 and 7 A $dm^{-2}$ current densities.

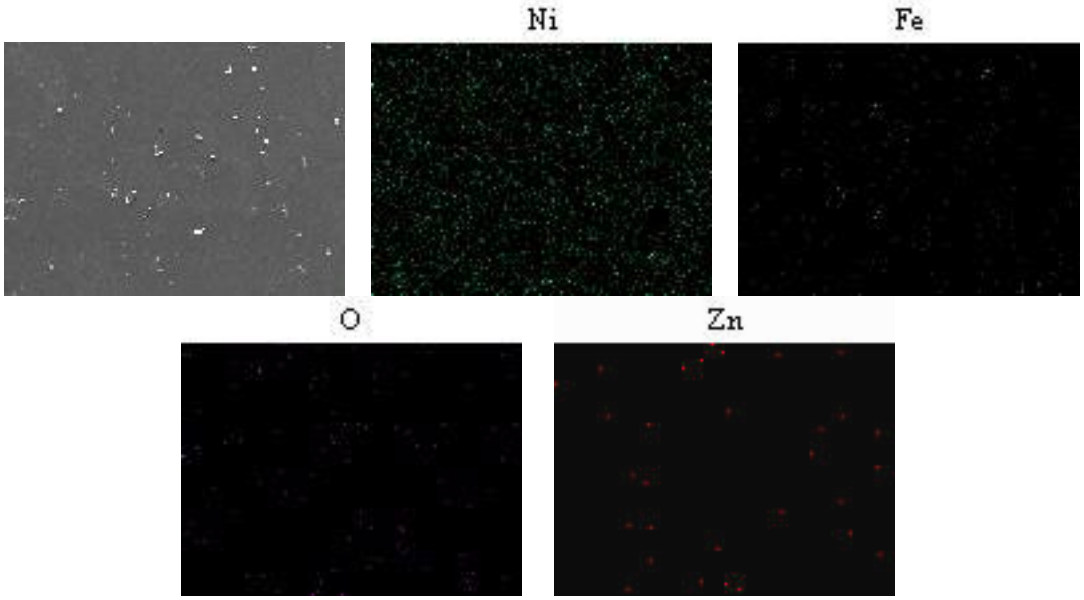


Figure 5.13 Mapping images of Ni-ZnO nanocomposite coatings with 50 nm sized and 1 gr/lt concentration ZnO nanoparticles.

## 5.5 Characterization of Electrodeposited Ni-$Cr_2O_3$ Nanocomposite Coatings

The phase structure of the Ni-$Cr_2O_3$ nanocomposite coatings was studied using X-ray diffractometry. Fig. 5.14 shows that XRD patterns of Ni-$Cr_2O_3$ nanocomposite coatings which synthesized different operating conditions. The diffraction peaks at 44.48°, 51.83° and 76.35° correspond to (111), (200) and (220) crystalline planes of Ni, respectively (Li, Hou & Liang, 2016). No $Cr_2O_3$ peaks could be seen from Ni-$Cr_2O_3$ nanocomposite coatings, probably due to the low quantity and highly dispersive form of the nanoparticles (Wang et al., 2015).

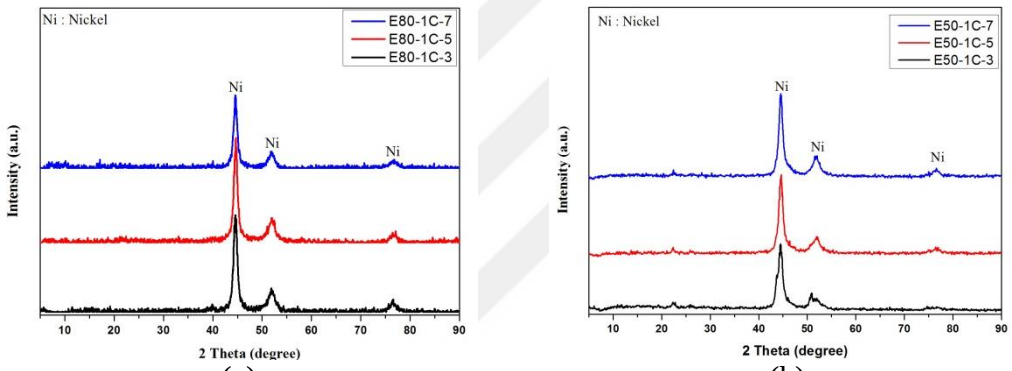


Figure 5.14 X-ray θ-2θ scans of Ni-$Cr_2O_3$ nanocomposite coatings with $Cr_2O_3$ nanoparticles (a) 80 nm sized and 1 gr/lt concentration, (b) 50 nm sized and 1 gr/lt concentration electrodeposited at 3, 5 and 7 A $dm^{-2}$ current densities.

Fig. 5.15 exemplifies SEM images of surface of the Ni-$Cr_2O_3$ nanocomposite coating electrodeposited from the bath containing 1 g/l and 3 g/l $Cr_2O_3$ nanoparticles. The obtained $Cr_2O_3$ nanoparticles are distributed in the deposit as white spherical globules. The distribution of the $Cr_2O_3$ nanoparticles on the cathode surface increases with increasing amount of suspended $Cr_2O_3$ in the bath (Hassan & Hamid, 2011). Hassan and Hamid prepared nanocomposite coatings of Ni-$Cr_2O_3$ supported on carbon electrodes by electrodeposition technique. According to their study, the shape of Ni crystallites is regular pyramidal structure. Incorporation of $Cr_2O_3$ nanopaticles has modified the surface morphology of nickel matrix. It is clear from the SEM images that the presence of $Cr_2O_3$ nanoparticles into the deposit reduces the size of Ni grains, due to the distribution of $Cr_2O_3$ particles on the boundaries of Ni grains, which restricts

the growth of Ni grains in the deposition process and results in surfaces of fine grains (Hassan & Hamid, 2011).

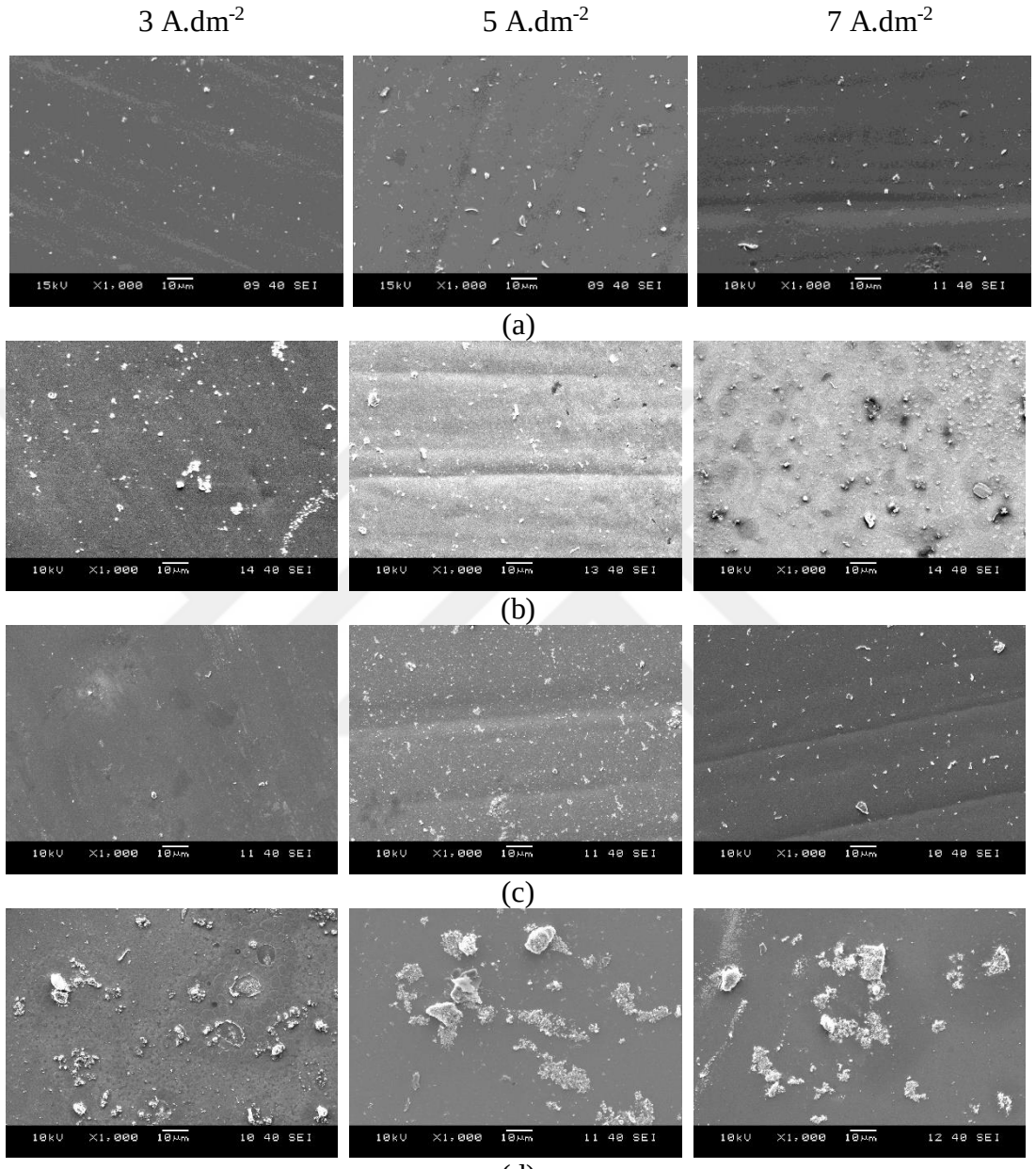


Figure 5.15 Surface morphologies of (a) pure nickel and Ni- $Cr_2O_3$ nanocomposite coatings with $Cr_2O_3$ nanoparticles (b) 80 nm sized and 1 gr/lt concentration, (c) 50 nm sized and 1 gr/lt concentration and (d) 50 nm sized and 3 gr/lt concentration electrodeposited at 3, 5 and 7 A $dm^{-2}$ current densities.

Figure 5.16 shows the results of the SEM-EDS mapping analysis study to determine the distribution of $Cr_2O_3$ nanoparticles by nanocomposite coatings. In addition the distribution of $Cr_2O_3$ particles is uniformly homogenous in all the samples.

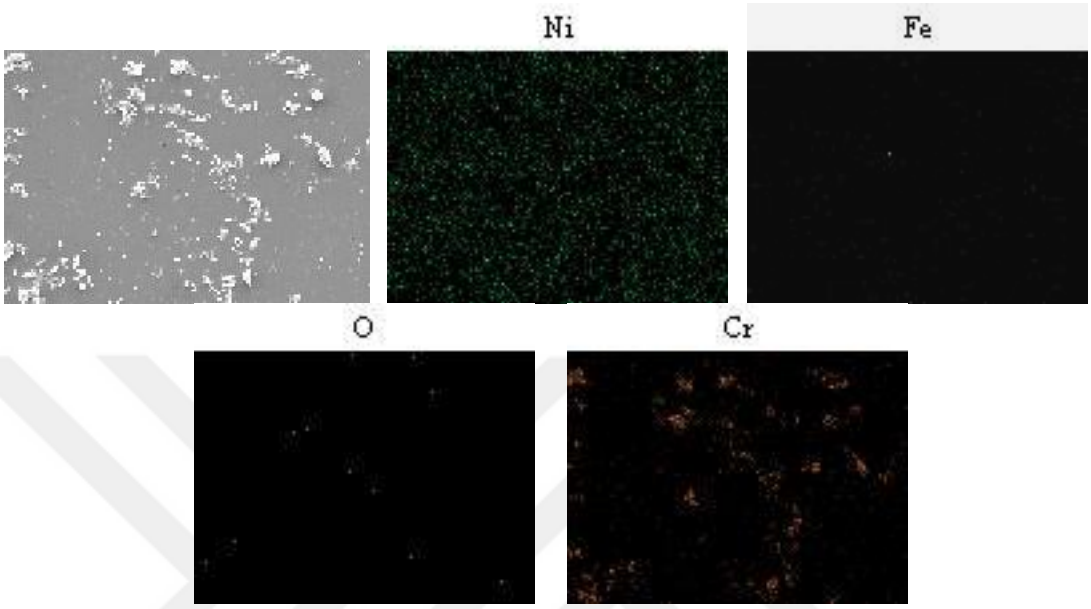


Figure 5.16 Mapping images of Ni-$Cr_2O_3$ nanocomposite coatings with 50 nm sized and 1 gr/lt concentration $Cr_2O_3$ nanoparticles.

## 5.6 Nanoindentation Studies of Ni Matrix Nanocomposite Coatings

The goal of the majority of nanoindentation tests is to extract elastic modulus and hardness of the specimen material from load-displacement measurements. Conventional indentation hardness tests involve the measurement of the size of a residual plastic impression in the specimen as a function of the indenter load. This provides a measure of the area of contact for a given indenter load. In a nanoindentation test, the size of the residual impression is often only a few microns and this makes it very difficult to obtain a direct measure using optical techniques. In nanoindentation testing, the depth of penetration beneath the specimen surface is measured as the load is applied to the indenter. The known geometry of the indenter then allows the size of the area of contact to be determined. The procedure also allows for the modulus of the specimen material to be obtained from a measurement of the "stiffness" of the contact, that is, the rate of change of load and depth.

Wu and his colleagues investigated microstructure, hardness and deformation behaviors of Zr-Si-N nanocomposite coatings with 0-20.9 at.% Si. According to their results an excessive addition of Si produces a detrimental effect on both the coating hardness and elastic modulus. Nanoindentation induced plastic deformation of the Si-free coating occurs by dislocation glides, microcrack initiation and propagation along the columnar grain boundaries. The microcrack propagation is considered to be the primary factor deteriorating the coating hardness (Wu, Qi, Wei, Zhang & Wang, 2016).

Deyab and his colleagues investigated mechanical and corrosion properties of epoxy/metal phthalocyanines nanocomposites on carbon steel. The results indicate that NiPc/Epoxy nanocomposite is the highest in elastic modulus and hardness than others (Deyab, De Riccardis & Mele, 2016).

Choi and his colleagues synthesized Zr-Si-N coatings with various Si contents by a hybrid coating system combining arc ion plating and d.c. magnetron sputtering techniques. According to their results the coatings with a Si content of 5.8 at.% exhibited the maximum hardness (H), Young's modulus (E), and H/E* values of 33 GPa, 265 GPa, and 0.12, respectively. The solid solution strengthening and grain boundary hardening were considered to be responsible for the enhanced mechanical properties of the Zr–Si–N coatings (Choi et al., 2014).

In our study, pure Ni and Ni-$TiO_2$ nanocomposite coatings were selected to determine required load level for nanoindentation measurements. First of all, surface roughness and coating thickness of the samples were measured and results are given in Table 5.4. Due to the reason that pure Ni coating has lowest surface roughness and coating thickness, values, loads from 10 mN to 200 mN was applied to pure Ni coating. Load-displacement curves of pure Ni coating are shown in Fig 5.17. The maximum indentation depth at 150 mN applied load is less than 1% of the coating thickness, excluding any influence of the substrate on the experimental results (Wang et. al., 2016). In order to minimize these effects, a maximum load of 150 mN was applied for

measurements for all coatings. By applying the Oliver and Pharr approach the nanohardness (H) and elastic modulus (E) of the coatings were obtained (Oliver & Pharr, 1992). E and H values were average of 262.67 GPa and 8.52 GPa. Measurements performed by applying the indenter on different areas of each investigated surface.

Table 5.4 Surface roughness and coating thickness of pure Ni and Ni nanocomposite coatings

| Sample | Surface Roughness ($R_a$) | Coating Thickness (µm) |
|---|---|---|
| Pure Ni | 0.0925 | 48.32 |
| E50-1T-3 | 0.2719 | 54.68 |
| E50-1T-5 | 0.3788 | 85.44 |
| E50-1T-7 | 0.4007 | 95.56 |
| E50-3T-3 | 0.2022 | 49.48 |
| E50-3T-5 | 0.2386 | 64.76 |
| E50-3T-7 | 0.9331 | 70.16 |

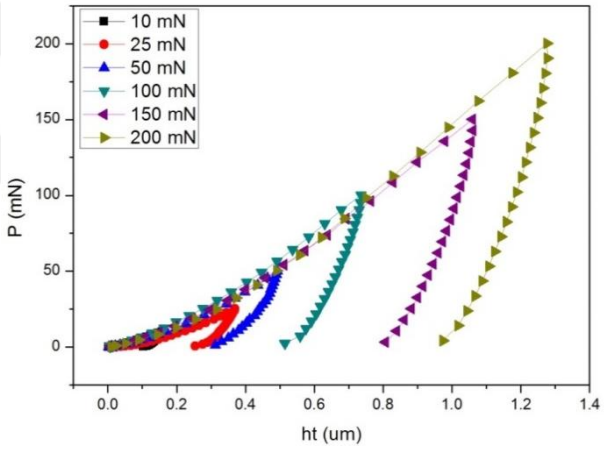


Figure 5.17 Nanoindentation studies of pure Ni coating.

The hardness of Ni-$TiO_2$ nanocomposite coatings and pure Ni coating are indicated in Fig. 5.18. It was found that the hardness values of Ni-$TiO_2$ nanocomposite coatings are higher than that of pure Ni coating prepared under the same condition and for a rising content of embedded $TiO_2$ nanoparticles in coating, an increase in the hardness was observed. It was observed that the hardness of E50-3T nanocomposite coatings are improved by increasing current density. Similar results are observed in literature. For example, Baghery and his colleagues prepared Ni-$TiO_2$ nanocomposite coatings with various contents of $TiO_2$ nanoparticles by electrodeposition in a Ni plating bath

containing $TiO_2$ nanoparticles to be codeposited. According to their results, The codeposited $TiO_2$ nanoparticles were uniformly distributed into Ni matrix improved mechanical properties of coating. The hardness of Ni-$TiO_2$ nanocomposite coating are improved by increasing of $TiO_2$ wt.% in coating (Baghery et al., 2010). Parida and his colleagues prepared $TiO_2$ dispersed nickel composite coatings by direct current deposition process on steel substrate from Watts bath to improve the surface mechanical property of nickel coating. For deagglomeration, Hexa decylpyridinium bromide (HPB) was used in varying quantity in plating bath as surfactant. From the results, hardness values were increased after incorporation of $TiO_2$ compared to pure nickel deposition. Due to soft orientation and less powder loading hardness increase is less pronounced in zero or 0.3 g/l surfactant added samples compared to 0.1 g/l surfactant added samples. Maximum hardness was reported with 0.3 g/l surfactant and 15 g/l $TiO_2$ in the bath.

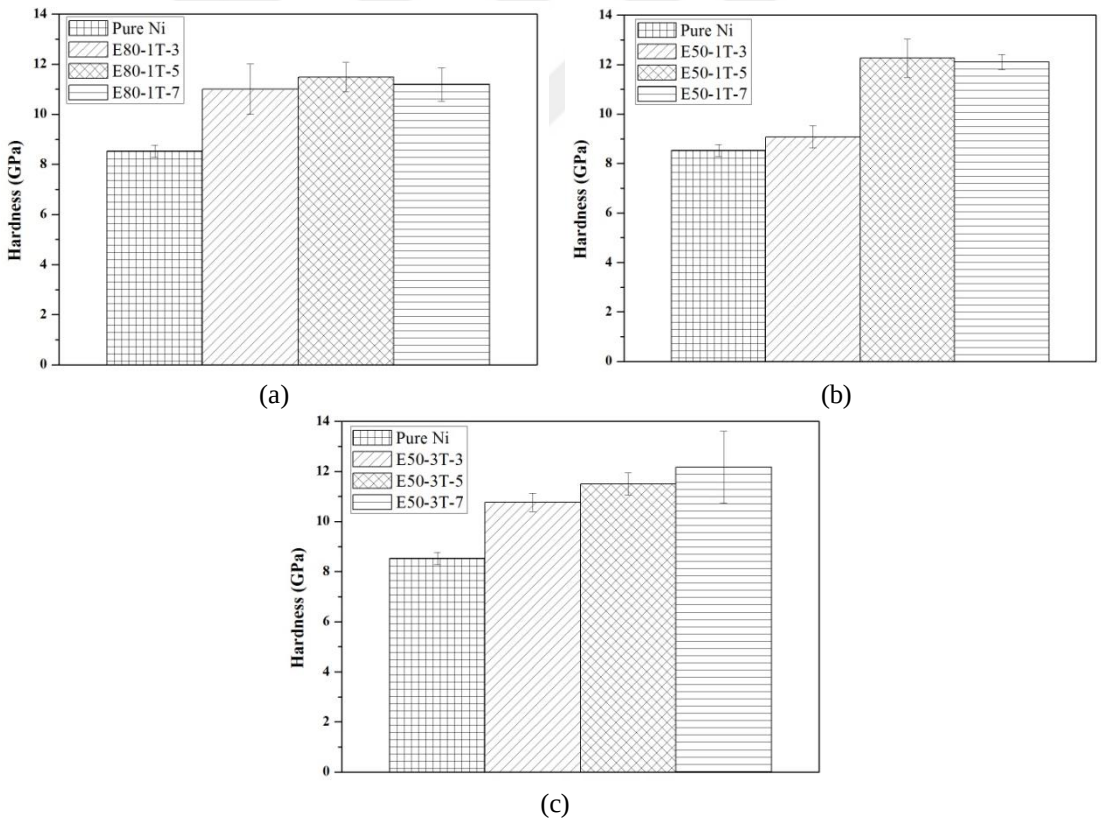


Figure 5.18 Comparative nanoindentation results of pure nickel and Ni-$TiO_2$ nanocomposite coatings with $TiO_2$ nanoparticles (a) 80 nm sized and 1 g/l concentration, (b) 50 nm sized and 1 g/l concentration and (c) 50 nm sized and 3 g/l concentration electrodeposited at 3, 5 and 7 A $dm^{-2}$ current densities.

Finally, Chen and Gao prepared Ni-$TiO_2$ composite coatings. According their study, Ni-$TiO_2$ nanocomposite coatings were electroplated by adding a transparent $TiO_2$ sol into the traditional electroplating Ni solution. Aim of their study was to investigate the effects of sol concentration on the hardness. From the results, the higher concentrations also led to higher contents of $TiO_2$ nanoparticles in the coating matrix. Simultaneously, the mechanical properties of the composite coatings improved steadily (Chen & Gao, 2010). Table 5.5 summarizes calculated mechanical parameters of pure Ni and Ni-$TiO_2$ nanocomposite coatings. Wear resistance is often correlated to mechanical parameters such as H/E and $H^3/E^2$ ratios, which provides simultaneous information about resistance to plastic deformation and elastic properties of materials (Chernogorova, Drozdova, Blinov & Bul'enkov, 2008; Musil, Kunc, Zeman & Polakova, 2002; Zhang, Wang & Nie, 2007). Musil and his colleagues investigated mechanical properties of hard and superhard nanocomposite coatings. According to their results the hard nanocomposite coatings exhibited the maximum hardness (H), Young's modulus (E), H/E and $H^3/E^2$ values of 46 GPa, 352 GPa, 0.13 and 0.78 respectively. The wear resistance of nanocomposite coatings is improved by increasing of H/E and $H^3/E^2$ ratios (Musil, Kunc, Zeman & Polakova, 2002).

Table 5.5 Mechanical properties of pure Ni and Ni-$TiO_2$ nanocomposite coatings

| **Coatings** | **H (GPa)** | **E (GPa)** | **H/E** | **$H^3/E^2$ (GPa)** |
|---|---|---|---|---|
| Pure Ni | 8.52 | 262.67 | 0.032 | 0.0090 |
| E80-1T-3 | 11.00 | 313.14 | 0.035 | 0.0136 |
| E80-1T-5 | 11.48 | 300.73 | 0.038 | 0.0167 |
| E80-1T-7 | 11.19 | 307.95 | 0.036 | 0.0148 |
| E50-1T-3 | 9.07 | 266.14 | 0.034 | 0.0105 |
| E50-1T-5 | 12.25 | 280.06 | 0.044 | 0.0234 |
| E50-1T-7 | 12.10 | 305.50 | 0.040 | 0.0190 |
| E50-3T-3 | 10.76 | 235.47 | 0.046 | 0.0225 |
| E50-3T-5 | 11.49 | 307.21 | 0.037 | 0.0161 |
| E50-3T-7 | 12.16 | 337.71 | 0.036 | 0.0158 |

The hardness of the pure Ni coating and Ni-ZnO nanocomposite coatings is given in Figure 5.19. Table 5.6 summarizes calculated mechanical properties of pure Ni and Ni-ZnO nanocomposite coatings. The results of the hardness suggest that the addition of ZnO nanoparticles in the coating does not have consistent to the hardness of the sample. For example, the hardness of E80-1Z-3 and E80-1Z-5 is lower than pure Ni.

On the other hand, the hardness of Ni-ZnO nanocomposite coating are improved by increasing of current density. Sharma and his colleagues prepared Ni-P-ZnO nanocomposite coating on the mild steel substrate by electroless technique. In their study, ZnO nanoparticles were synthesized by autocombustion method. According to their results, the hardness value is improved on incorporation of nanosize ZnO particles than the microsize particles into the Ni-P matrix (Sharma et al., 2016).

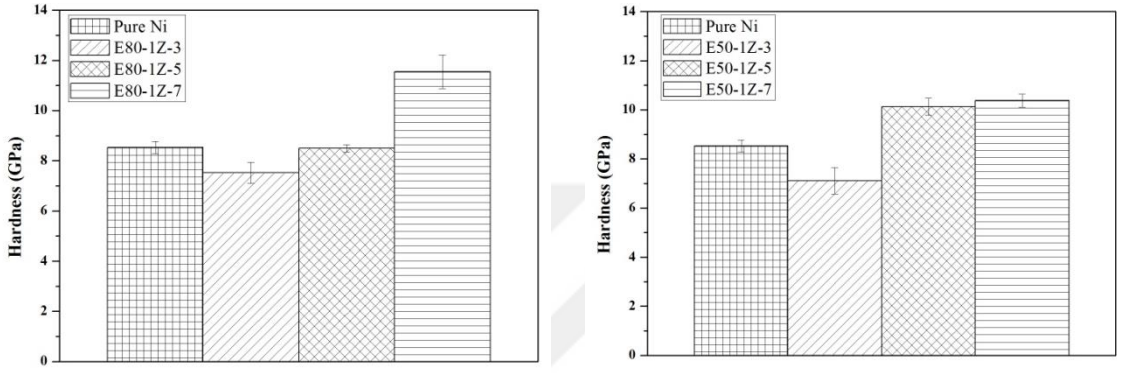


(a) (b)

Figure 5.19 Comparative nanoindentation results of pure nickel and Ni-ZnO nanocomposite coatings with ZnO nanoparticles (a) 80 nm sized and 1 g/l concentration, (b) 50 nm sized and 1 g/l concentration electrodeposited at 3, 5 and 7 A $dm^{-2}$ current densities.

Table 5.6 Mechanical properties of pure Ni and Ni-ZnO nanocomposite coatings

| **Coatings** | **H (GPa)** | **E (GPa)** | **H/E** | **$H^3/E^2$ (GPa)** |
|---|---|---|---|---|
| Pure Ni | 8.52 | 262.67 | 0.032 | 0.0090 |
| E80-1Z-3 | 7.51 | 296.08 | 0.025 | 0.0048 |
| E80-1Z-5 | 8.49 | 260.24 | 0.033 | 0.0090 |
| E80-1Z-7 | 11.53 | 329.48 | 0.035 | 0.0141 |
| E50-1Z-3 | 7.11 | 243.24 | 0.029 | 0.0061 |
| E50-1Z-5 | 10.12 | 290.98 | 0.035 | 0.0122 |
| E50-1Z-7 | 10.37 | 312.73 | 0.033 | 0.0114 |

The hardness of Ni–$Cr_2O_3$ nanocomposite coatings at different conditions and pure Ni coating is presented in Fig. 5.20. Table 5.7 summarizes calculated mechanical properties of pure Ni and Ni-$Cr_2O_3$ nanocomposite coatings. The results of the hardness suggest that the addition of $Cr_2O_3$ nanoparticles in the coating contributes significantly to the hardness of the sample. From the results, generally Ni-$Cr_2O_3$ nanocomposite coatings which synthesized at 3 A.$dm^{-2}$ have highest hardness value. Similar results are observed in literature. Srivastava and his colleagues prepared Ni-

$Cr_2O_3$ nanocomposite coatings by the electrodeposition method using sulphamate electrolyte. According to their study, the mechanical property like hardness of nanocomposite coatings was studied. From the results, the incorporation of $Cr_2O_3$ particles enhanced the mechanical properties of Ni matrix (Srivastava et al., 2010). In another work, Abdel Hamid and El-Sheikh produced Ni-$Cr_2O_3$ nanocomposite coatings by conventional electroplating technique. In their study, influence of nano-$Cr_2O_3$ concentrations in Ni matrix was investigated. According to their results, the incorporation of $Cr_2O_3$ particles with nickel matrix confers greatly increased values of hardness (Hamid & El-Sheikh, 2013).

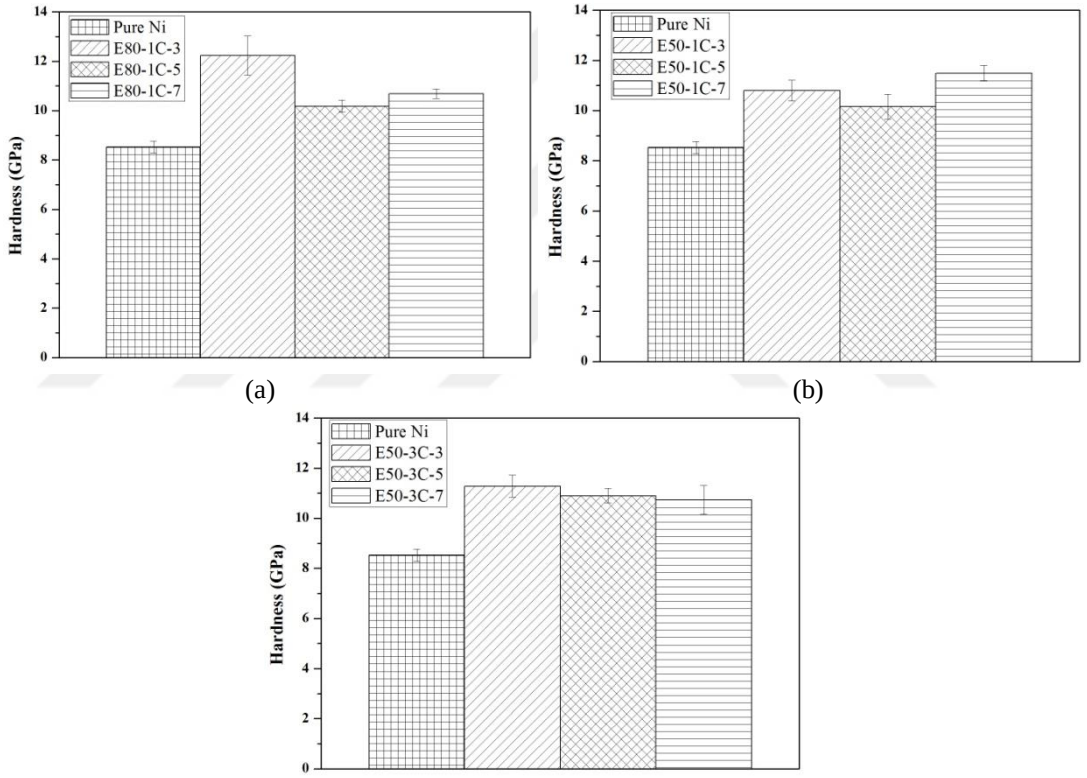


Figure 5.20 Comparative nanoindentation results of pure nickel and Ni-$Cr_2O_3$ nanocomposite coatings with $Cr_2O_3$ nanoparticles (a) 80 nm sized and 1 g/l concentration, (b) 50 nm sized and 1 g/l concentration and (c) 50 nm sized and 3 g/l concentration electrodeposited at 3, 5 and 7 A $dm^{-2}$ current densities.

Table 5.7 Mechanical properties of pure Ni and Ni-$Cr_2O_3$ nanocomposite coatings

| **Coatings** | **H (GPa)** | **E (GPa)** | **H/E** | **$H^3/E^2$ (GPa)** |
|---|---|---|---|---|
| Pure Ni | 8.52 | 262.67 | 0.032 | 0.0090 |
| E80-1C-3 | 12.23 | 330.41 | 0.037 | 0.0168 |
| E80-1C-5 | 10.18 | 315.79 | 0.032 | 0.0106 |
| E80-1C-7 | 10.68 | 319.53 | 0.033 | 0.0119 |
| E50-1C-3 | 10.79 | 267.59 | 0.040 | 0.0175 |
| E50-1C-5 | 10.15 | 301.59 | 0.034 | 0.0115 |
| E50-1C-7 | 11.48 | 305.73 | 0.038 | 0.0162 |
| E50-3C-3 | 11.27 | 309.66 | 0.036 | 0.0149 |
| E50-3C-5 | 10.89 | 275.51 | 0.040 | 0.0170 |
| E50-3C-7 | 10.73 | 198.89 | 0.054 | 0.0312 |

Finally, from the results of hardness and elastic modulus of pure Ni and Ni based nanocomposite coatings, it was observed that the incorporation of nanoparticles enhanced the wear resistance of Ni matrix. Nevertheless, E80-1Z-3 and E50-1Z-3 coatings have lower wear resistance than pure Ni coating.

# CHAPTER SIX
# CONCLUSION

In the present work, firstly $TiO_2$, ZnO and $Cr_2O_3$ nanoparticles were synthesized via sol-gel method. Then, Ni based nanocomposite coatings were electrodeposited on steel substrates from Watts bath by electrodeposition method. The effects of current density, particle size and particle concentration on the surface morphology and mechanical properties of the nanocomposite coatings were investigated.

Particle size distributions of nanoparticles were measured using Zeta-sizer. Crystalline structures of nanoparticles and coatings were analyzed using X-Ray Diffraction (XRD). Morphological characteristics of coatings were examined using Scanning Electron Microscopy (SEM). Nanoindentation measurements of the coatings were performed using a nanoindentation system.

The following conclusions are obtained from the experimental work:

- According to XRD results, $TiO_2$, ZnO and $Cr_2O_3$ nanoparticles are composed of anatase, zincite and eskolaite phases, respectively.

- All nanoparticles with different sizes were synthesized using sol-gel method. The average particle sizes of nanoparticles were measured ~50 and ~80 nm.

- According to XRD results, the Ni phase was observed in pure Ni and Ni based nanocomposite coatings, indicating that the particle addition did not significantly change the phase structure of coatings.

- SEM and mapping images of coatings shows that the codeposited nanoparticles were uniformly distributed into Ni matrix.

- Based on indentation results of pure Ni and Ni based nanocomposite coatings, the mechanical properties of Ni-$TiO_2$ and Ni-$Cr_2O_3$ nanocomposite coatings were better than pure Ni coating.

## REFERENCES


Aghaie-Khafri, M., & Lafdani, M. K. (2012). A novel method to synthesize $Cr_2O_3$ nanopowders using edta as a chelating agent. *Powder Technology, 222*, 152-159.

Ahmad, Y. H., & Mohamed, A. (2014). Electrodeposition of nanostructured nickel-ceramic composite coatings: A review. *International Journal of Electrochemical Sciences, 9*, 1942-1963.

Ahmed, W., & Jackson, M. J. (2014). Nanotechnology to nanomanufacturing. W. Ahmed, (Ed.), *Emerging Nanotechnologies for Manufacturing* (1-15). Burlington: William Andrew.

Alagarasi, A. (2011). *Introduction to nanomaterials*. Retrieved June 8, 2016, from http://nccr.iitm.ac.in/2011.pdf.

Alias, S., Ismail, A., & Mohamad, A. (2010). Effect of ph on ZnO nanoparticle properties synthesized by sol–gel centrifugation. *Journal of Alloys and Compounds, 499* (2), 231-237.

Armentano, I., Dottori, M., Fortunati, E., Mattioli, S., & Kenny, J. (2010). Biodegradable polymer matrix nanocomposites for tissue engineering: A review. *Polymer Degradation and Stability, 95* (11), 2126-2146.

Ba-Abbad, M. M., Kadhum, A. A. H., Mohamad, A. B., Takriff, M. S., & Sopian, K. (2013). The effect of process parameters on the size of ZnO nanoparticles synthesized via the sol–gel technique. *Journal of Alloys and Compounds, 550*, 63-70.

Bagheri, S., Shameli, K., & Abd Hamid, S. B. (2012). Synthesis and characterization of anatase titanium dioxide nanoparticles using egg white solution via sol-gel method. *Journal of Chemistry, 2013*.

Baghery, P., Farzam, M., Mousavi, A. ,& Hosseini, M. (2010). Ni–$TiO_2$ nanocomposite coating with high resistance to corrosion and wear. *Surface and Coatings Technology, 204* (23), 3804-3810.

Baker, C., Shah, S. I., & Hasanain, S. (2004). Magnetic behavior of iron and iron-oxide nanoparticle/polymer composites. *Journal of Magnetism and Magnetic Materials, 280* (2), 412-418.

Bakhit, B., & Akbari, A. (2013). Synthesis and characterization of Ni–Co/SiC nanocomposite coatings using sediment co-deposition technique. *Journal of Alloys and Compounds, 560*, 92-104.

Berkovich, E. (1951). Three-faceted diamond pyramid for micro-hardness testing. *Industrial Diamond Review, 11* (127), 129-133.

Berthelot, J. M. (2012). *Composite materials: Mechanical behavior and structural analysis*. New York: Springer Science & Business Media.

Brinker, C. (1988). Hydrolysis and condensation of silicates: Effects on structure. *Journal of Non-Crystalline Solids, 100* (1), 31-50.

Brinker, C., Raman, N., Logan, M., Sehgal, R., Assink, R. A., Hua, D. W. et al., (1995). Structure-property relationships in thin films and membranes. *Journal of Sol-Gel Science and Technology, 4* (2), 117-133.

Brinker, C. J., & Scherer, G. W. (2013). *Sol-gel science: The physics and chemistry of sol-gel processing*. San Diego: Academic Press.

Buzea, C., Pacheco, I. I., & Robbie, K. (2007). Nanomaterials and nanoparticles: Sources and toxicity. *Biointerphases, 2* (4), 17-71.

Callister, W. D., & Rethwisch, D. G. (2007). *Materials science and engineering: An introduction*. New York: Wiley.

Camargo, P. H. C., Satyanarayana, K. G., & Wypych, F. (2009). Nanocomposites: Synthesis, structure, properties and new application opportunities. *Materials Research, 12* (1), 1-39.

Cao, G. (2004). *Nanostructure and nanomaterials: Synthesis, properties and applications* (2nd ed.). London: Imperial College Press.

Casati, R., & Vedani, M. (2014). Metal matrix composites reinforced by nano-particles: A review. *Metals, 4* (1), 65-83.

Chen, W., & Gao, W. (2010). Sol-enhanced electroplating of nanostructured Ni-$TiO_2$ composite coatings- the effects of sol concentration on the mechanical and corrosion properties. *Electrochimica Acta, 55* (22), 6865-6871.

Chernogorova, O., Drozdova, E., Blinov, V., & Bul'enkov, N. (2008). Structure and properties of the superelastic and hard carbon particles reinforcing wear-resistant composite materials obtained from mixtures of iron and fullerene powders under pressure. *Nanotechnologies in Russia, 3* (5-6), 344-351.

Choi, H., Jang, J., Zhang, T., Kim, J. H., Park, I. W., & Kim, K. H. (2014). Effect of Si addition on the microstructure, mechanical properties and tribological properties of Zr–Si–N nanocomposite coatings deposited by a hybrid coating system. *Surface and Coatings Technology*, *259*, 707-713.

Conway, B. E. (1952). *Electrochemical data*. Santa Barbara: Praeger.

Conway, B. E. (1965). *Theory and principles of electrode processes*. New York: Ronald Press.

Creasey, D. J., Heard, D. E., Pilling, M. J., Whitaker, B. J., Berzins, M., & Fairlie, R. (1997). Visualisation of a supersonic free-jet expansion using laser-induced fluorescence spectroscopy: application to the measurement of rate constants at ultralow temperatures. *Applied Physics B, 65* (3), 375-391.

Dalvandi, M., & Ghasemi, B. (2013). Synthesis of titanium dioxide nano-powder via sol-gel method at ambient temperature. *Journal of Sol-Gel Science and Technology, 66* (1), 68-72.

Dennis, J. K., & Such, T. E. (1993). *Nickel and chromium plating* (3rd ed.). Cambridge: Woodhead Publishing.

Dermenci, K. B., Genc, B., Ebin, B., Hanci, T., & Gürmen, S. (2014). Photocatalytic studies of Ag/ZnO nanocomposite particles produced via ultrasonic spray pyrolysis method. *Journal of Alloys and Compounds, 586,* 267-273.

Deyab, M., De Riccardis, A., & Mele, G. (2016). Novel epoxy/metal phthalocyanines nanocomposite coatings for corrosion protection of carbon steel. *Journal of Molecular Liquids, 220*, 513-517.

Di Bari, G. A. (2000). Electrodeposition of nickel. *Modern Electroplating, 5*, 79-114.

Doeuff, S., Henry, M., Sanchez, C., & Livage, J. (1987). Hydrolysis of titanium alkoxides: modification of the molecular precursor by acetic acid. *Journal of Non-Crystalline Solids, 89* (1), 206-216.

Du, L., Xu, B., Dong, S., Yang, H., & Tu, W. (2004). Study of tribological characteristics and wear mechanism of nano-particle strengthened nickel-based composite coatings under abrasive contaminant lubrication. *Wear, 257* (9), 1058-1063.

Dunn, B., Farrington, G. C., & Katz, B. (1994). Sol-gel approaches for solid electrolytes and electrode materials. *Solid State Ionics, 70,* 3-10.

Faga, M., Gautier, G., Calzavarini, R., Perucca, M., Boot, E. A., Cartasegna, F. et al., (2007). AlSiTiN nanocomposite coatings developed via arc cathodic pvd: Evaluation of wear resistance via tribological analysis and high speed machining operations. *Wear, 263* (7), 1306-1314.

Feng, Q., Li, T., Yue, H., Qi, K., Bai, F., & Jin, J. (2008). Preparation and characterization of nickel nano-$Al_2O_3$ composite coatings by sediment co-deposition. *Applied Surface Science, 254* (8), 2262-2268.

Fischer-Cripps, A. C. (2009). *The ibis handbook of nanoindentation*. Forestville: Fischer-Cripps Laboratories.

Freitas, M., & Garcia, E. (2007). Electrochemical recycling of cobalt from cathodes of spent lithium-ion batteries. *Journal of Power Sources, 171* (2), 953-959.

Garcia, E. M., Lins, V. F., & Matencio, T. (2013). Metallic and oxide electrodeposition. *Modern Surface Engineering Treatments, 5*, 12-22. Retrieved May 8, 2016, from InTech database.

Gorrasi, G., Vittoria, V., Murariu, M., Ferreira, A. D. S., Alexandre, M., & Dubois, P. (2008). Effect of filler content and size on transport properties of water vapor in polylactide/calcium sulfate composites. *Biomacromolecules, 9* (3), 984-990.

Gvishi, R., Narang, U., Ruland, G., Kumar, D. N., & Prasad, P. N. (1997). Novel, organically doped, sol–gel-derived materials for photonics: multiphasic nanostructured composite monoliths and optical fibers. *Applied Organometallic Chemistry, 11* (2), 107-127.

Hamid, Z. A., & El-Sheikh, S. (2013). Enhancement the properties of Ni compisite electroplated using nano-chromium oxide powder. *Journal of Metallurgical Engineering, 2* (2), 71-79.

Hassan, H., & Hamid, Z. A. (2011). Electrodeposited Ni-$Cr_2O_3$ nanocomposite anodes for ethanol electrooxidation. *International Journal of Hydrogen Energy, 36* (8), 5117-5127.

Holister, P., Weener, J., Vas, C., & Harper, T. (2003). *Nanoparticles; technology white papers* Cientifica.

Horikoshi, S., & Serpone, N. (2013). Introduction to nanoparticles. *Microwaves in Nanoparticle Synthesis: Fundamentals and Applications*, 1-24.

Hou, K., Ger, M., Wang, L., & Ke, S. (2002). The wear behaviour of electro-codeposited Ni-SiC composites. *Wear, 253* (9), 994-1003.

Hou, X., Choy, K. L., Brun, N., & Serín, V. (2013). Nanocomposite coatings codeposited with nanoparticles using aerosol-assisted chemical vapour deposition. *Journal of Nanomaterials, 2013*, 1-8.

Hussain, F., Hojjati, M., Okamoto, M., & Gorga, R. E. (2006). Polymer-matrix nanocomposites, processing, manufacturing, and application: An overview. *Journal of Composite Materials, 40* (17), 1511-1575.

Instruments, M. (2004). *Zetasizer nano series user manual*. Worcester: Malvern Instruments.

Karimian, R., Piri, F., & Davarpanah, S. J. (2014). Synthesis of zinc oxide and chromium (iii) oxide nanoparticles with diverse. *Journal of Applied Biotechnology Reports, 1* (2), 73-76.

Khalil, M., Eldin, T. A. S., Hassan, H., El-Sayed, K., & Hamid, Z. A. (2015). Electrodeposition of Ni-GNS-$TiO_2$ nanocomposite coatings as anticorrosion film for mild steel in neutral environment. *Surface and Coatings Technology, 275*, 98-111.

Kim, D. W., Shin, S. I., Lee, J. D., & Oh, S. G. (2004). Preparation of chromia nanoparticles by precipitation-gelation reaction. *Materials Letters, 58* (12), 1894-1898.

Koch, C. C. (2006). *Nanostructured materials: Processing, properties and applications* (2nd ed.). Burlington: William Andrew.

Kolekar, T., Yadav, H., Bandgar, S., & Deshmukh, P. (2011). Synthesis by sol–gel method and characterization of ZnO nanoparticles. *Indian Streams Research Journal, 1* (1), 1-4.

Kumar, A., Malik, A. K., Tewary, D. K., & Singh, B. (2008). A review on development of solid phase microextraction fibers by sol-gel methods and their applications. *Analytica Chimica Acta, 610* (1), 1-14.

Lajevardi, S., & Shahrabi, T. (2010). Effects of pulse electrodeposition parameters on the properties of Ni-$TiO_2$ nanocomposite coatings. *Applied Surface Science, 256* (22), 6775-6781.

Levy, D., & Esquivias, L. (1995). Sol-gel processing of optical and electrooptical materials. *Advanced Materials, 7* (2), 120-129.

Li, R., Hou, Y., & Liang, J. (2016). Electro-codeposition of Ni-$SiO_2$ nanocomposite coatings from deep eutectic solvent with improved corrosion resistance. *Applied Surface Science, 367*, 449-458.

Lin, C., Lee, C., Chang, C., & Chang, C. (2006). Annealing behavior of electrodeposited Ni-$TiO_2$ composite coatings. *Surface and Coatings Technology, 200* (12), 3690-3697.

Liu, L., & Xu, J. (2011). A study of the erosion-corrosion behavior of nano-$Cr_2O_3$ particles reinforced Ni-based composite alloying layer in aqueous slurry environment. *Vacuum, 85* (6), 687-700.

Mackenzie, J. D., & Ulrich, D. R. (1988). *Ultrastructure processing of advanced ceramics*. New York: Wiley.

Mahshid, S., Ghamsari, M. S., Askari, M., Afshar, N., & Lahuti, S. (2006). Synthesis of $TiO_2$ nanoparticles by hydrolysis and peptization of titanium isopropoxide solution. *Semiconductor Physics, Quantum Electronics & Optoelectronics, 9* (2), 65-68.

Max, S. (1934). *Formation of dense, highly lustrous and impervious deposits of nickel.* Retrieved June 11, 2016, from http://www.google.com/patents/US1972693

Melnik, A., & Shagalina, O. (2011). *History of nanotechnology*. Retrieved May 5, 2016, from http://conf.sfu-kras.ru/sites/mn2011/thesis/s22/s22_024.pdf.

Musil, J., Kunc, F., Zeman, H., & Polakova, H. (2002). Relationships between hardness, young's modulus and elastic recovery in hard nanocomposite coatings. *Surface and Coatings Technology, 154* (2), 304-313.

Nikulin, I., Kipelova, A., Malopheyev, S., & Kaibyshev, R. (2012). Effect of second phase particles on grain refinement during equal-channel angular pressing of an Al–Mg–Mn alloy. *Acta Materialia, 60* (2), 487-497.

Nogami, M., & Moriya, Y. (1980). Glass formation through hydrolysis of $Si(OC_2H_5)_4$ with $NH_4OH$ and HCl solution. *Journal of Non-Crystalline Solids, 37* (2), 191-201.

Oliver, W. C., & Pharr, G. M. (1992). An improved technique for determining hardness and elastic modulus using load and displacement sensing indentation experiments. *Journal of Materials Research, 7* (06), 1564-1583.

Ozmetin, A., Sahin, O., Ongun, E., & Kuru, M. (2015). Mechanical characterization of $MgB_2$ thin films using nanoindentation technique. *Journal of Alloys and Compounds, 619*, 262-266.

Pandey, R. K., Chandra, S., & Sahu, S. (1996). *Handbook of semiconductor electrodeposition*. Florida: CRC Press.

Parida, G., Chaira, D., Chopkar, M., & Basu, A. (2011). Synthesis and characterization of Ni-$TiO_2$ composite coatings by electro-co-deposition. *Surface and Coatings Technology*, *205* (21), 4871-4879.

Parsons, R. (1959). *Handbook of electrochemical data*. London: Butterworths.

Pierre, A. C. (2013). *Introduction to sol-gel processing*. Berlin: Springer Science & Business Media.

Qiao, S., Liu, J., & Lu, G. (2011). Synthetic chemistry of nanomaterials. Q. Huo, (Ed.). *Modern inorganic synthetic chemistry* (479-506). Amsterdam: Elsevier.

Rajput, N. (2015). Methods of preparation of nanoparticles-a review. *International Journal of Advances in Engineering & Technology*, *7* (6), 1806.

Roehl, E., & Wesley, W. (1950). Notes on nickel plating from a fluoborate bath. *Plating*, *37*, 142.

Rose, I., & Whittington, C. (2002). *Nickel plating handbook*. Finland: OM Group, Espoo.

Roy, R., Roy, R. A., & Roy, D. M. (1986). Alternative perspectives on "quasi-crystallinity": Non-uniformity and nanocomposites. *Materials Letters, 4* (8), 323-328.

Rusu, D., Cojocaru, P., Magagnin, L., Gheorghies, C., & Cârâc, G. (2010). Study of Ni-$TiO_2$ nanocomposite coating prepared by electrochemical deposition. *Journal of Optoelectronics and Advanced Materials, 12* (12), 2419-2422.

Sadiku-Agboola, O., Sadiku, E., Ojo, O., Akanji, O., & Biotidara, O. (2011). Influence of operation parameters on metal deposition in bright nickel-plating process. *Portugaliae Electrochimica Acta, 29* (2), 91-100.

Saha, R., & Khan, T. (2010). Effect of applied current on the electrodeposited Ni-$Al_2O_3$ composite coatings. *Surface and Coatings Technology, 205* (3), 890-895.

Salamanca-Buentello, F., Persad, D. L., Martin, D. K., Daar, A. S., & Singer, P. A. (2005). Nanotechnology and the developing world. *PLOS Medicine, 2* (5).

Scherer, G. W., & Brinker, C. J. (1990). *Sol-gel science: The physics and chemistry of sol-gel processing*. New York: Academic.

Schodek, D. L., Ferreira, P., & Ashby, M. F. (2009). *Nanomaterials, nanotechnologies and design: An introduction for engineers and architects*. London: Butterworths.

Schubert, U. (1994). Catalysts made of organic-inorganic hybrid materials. *New Journal of Chemistry, 18* (10), 1049-1058.

Schwartz, R. W. (1997). Chemical solution deposition of perovskite thin films. *Chemistry of Materials, 9* (11), 2325-2340.

Sharma, S., Sharma, S., Sharma, A., & Agarwala, V. (2016). Co-deposition of synthesized ZnO nanoparticles into Ni-P matrix using electroless technique and their corrosion study. *Journal of Materials Engineering and Performance*, 1-11.

Singh, L. P., Bhattacharyya, S. K., Kumar, R., Mishra, G., Sharma, U., Singh, G. et al., (2014). Sol-gel processing of silica nanoparticles and their applications. *Advances in Colloid and Interface Science, 214*, 17-37.

Singh, N. (2012). Effect of ageing in structural properties of ZnO nanoparticles with ph variation for application in solar cells. *The Open Renewable Energy Journal*, *5*, 15-18.

Srivastava, M., Balaraju, J., Ravishankar, B., & Rajam, K. (2010). Improvement in the properties of nickel by nano-$Cr_2O_3$ incorporation. *Surface and Coatings Technology*, *205* (1), 66-75.

Thakur, A., & Gangopadhyay, S. (2016). State-of-the-art in surface integrity in machining of nickel-based super alloys. *International Journal of Machine Tools and Manufacture, 100*, 25-54.

Thiemig, D., & Bund, A. (2008). Characterization of electrodeposited Ni-$TiO_2$ nanocomposite coatings. *Surface and Coatings Technology, 202* (13), 2976-2984.

Tolochko, N. (2009). *History of nanotechnology*. Retrieved July 17, 2016, from http://www.eolss.net/sample-chapters/c05/e6-152-01.pdf.

Vafaee, M., & Ghamsari, M. S. (2007). Preparation and characterization of ZnO nanoparticles by a novel sol–gel route. *Materials Letters, 61* (14), 3265-3268.

Vandaele, K. (2011). *$YBa_2Cu_3O_7$ coatings based on trifluoro-acetic acid precursors*. Retrieved August 9, 2016, from http://lib.ugent.be /fulltxt/ RUG01/ 001/787/456/ RUG01001787456_2012_0001_AC.pdf.

Vasilache, T., Gutt, S., Sandu, I., Vasilache, V., Gutt, G., Risca, M. et al., (2010). Electrochemical mechanism of nickel and zinc-nickel alloy electrodeposition. *Recent Patents on Corrosion Science, 2*, 1-5.

Wang, Q., Cao, Q., Wang, X., Jing, B., Kuang, H., & Zhou, L. (2013). A high-capacity carbon prepared from renewable chicken feather biopolymer for supercapacitors. *Journal of Power Sources, 225*, 101-107.

Wang, Q., Callisti, M., Greer, J., McKay, B., Milickovic, T. K., Zoikis-Karathanasis, A. et al., (2016). Effect of annealing temperature on microstructure, mechanical and tribological properties of nano-SiC reinforced Ni-P coatings. *Wear, 356*, 86-93.

Wang, Y., Tay, S. L., Wei, S., Xiong, C., Gao, W., Shakoor, R. et al., (2015). Microstructure and properties of sol-enhanced Ni-Co-$TiO_2$ nano-composite coatings on mild steel. *Journal of Alloys and Compounds, 649*, 222-228.

Watts, O., & Deverter, P. (1916). The protection of iron by electroplating. *Transactions of American Electrochemical Society, 30* (1).

Wesley, W., & Roehl, E. (1942). The electrodeposition of hard nickel. *Transactions of the Electrochemical Society, 82* (1), 37-53.

Wetchakun, N., Incessungvorn, B., Wetchakun, K., & Phanichphant, S. (2012). Influence of calcination temperature on anatase to rutile phase transformation in $TiO_2$ nanoparticles synthesized by the modified sol–gel method. *Materials Letters, 82*, 195-198.

Wheeler, J. M. (2009). *Nanoindentation under dynamic conditions.* Retrieved July 31, 2016, from http://www.repository.cam.ac.uk/handle/1810/218320.

Wolfbeis, O. S., Reisfeld, R., & Oehme, I. (1996). Sol-gels and chemical sensors. In *Optical and Electronic Phenomena in Sol-gel Glasses and Modern Application, 85,* 51-98.

Wu, Y., Wu, X., & Zhang, L. (2003). Preparation and microstructure characterization of Ni/$TiO_2$ nanocomposite. *China Particuology, 1* (6), 262-265.

Wu, Z., Qi, Z., Wei, B., Zhang, D., & Wang, Z. (2016). Understanding hardness evolution of Zr-Si-N nanocomposite coatings via investigating their deformation behaviors. *Journal of the European Ceramic Society, 36* (14), 3329-3339.

Young, S. K. (2002). *Overview of sol-gel science and technology*. Aberdeen: Army Research Laboratory.

Zeng, Z., Qiu, W., & Huang, Z. (2001). Solid-phase microextraction using fused-silica fibers coated with sol-gel-derived hydroxy-crown ether. *Analytical Chemistry, 73* (11), 2429-2436.

Zhang, P., Wang, L., & Nie, X. (2007). Tribological properties of a-C/Cr(N) coatings in micro-and nano-scales. *Surface and Coatings Technology, 201* (9), 5176-5181.